Chem Soc Rev

2008 Gold: Chemistry, Materials and Catalysis Issue

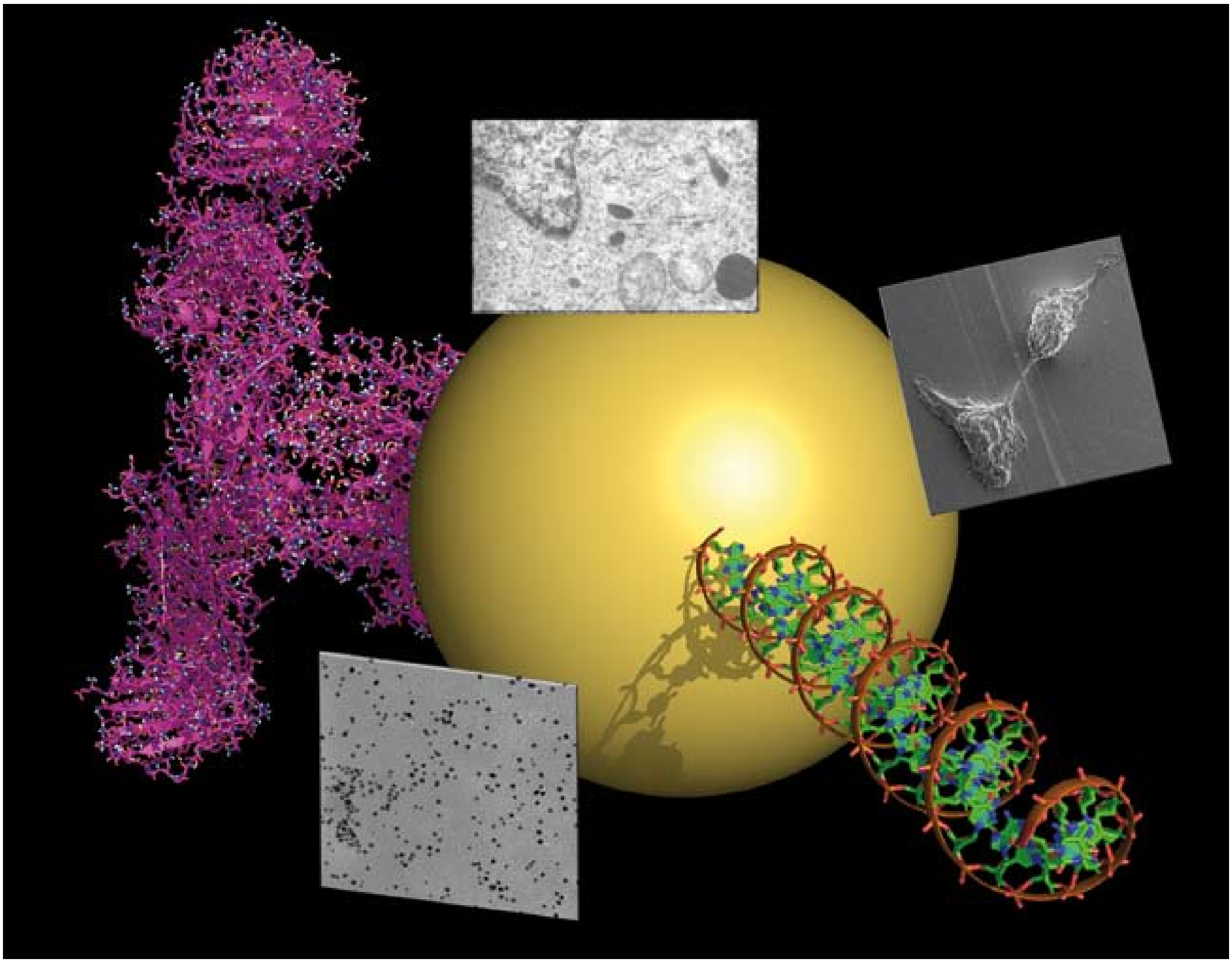

Theory and simulation in heterogeneous gold catalysis†

Rudy Coquet, Kara L. Howard and David J. Willock*

Received 30th June 2008
First published as an Advance Article on the web 30th July 2008
DOI: 10.1039/b707385m

This *critical review* covers the application of quantum chemistry to the burgeoning area of the heterogeneous oxidation by Au. We focus on the most established reaction, the oxidation of CO at low temperature. The review begins with an overview of the methods available comparing the treatment of the electron–electron interaction and relativistic effects. The structure of Au particles and their interaction with oxide reviews is then discussed in detail. Calculations of the adsorption and reaction of CO and O_2 are then considered and results from isolated and supported Au clusters compared (155 references).

1. Introduction

The discovery that nano-particulate gold can be an effective catalyst[1,2] has sparked a flurry of research in the area over the last two decades. Of particular interest is the low temperature oxidation of CO catalysed by supported Au particles. In addition to high activity for CO oxidation, supported Au catalysts can show remarkable selectivity. For example Au/Fe_2O_3 is able to oxidise CO in the presence of H_2, leading to the possibility of important technical applications in decontamination of hydrogen fuel cell feed streams.[3,4] Hutchings and Hashmi have recently produced a comprehensive review covering the remarkable range of reactions that are catalysed by Au in both the heterogeneous and homogeneous arenas.[5]

Theory, and in particular computational chemistry, has focused on understanding the origin of activity in the apparently simple CO oxidation reaction. Many suggestions have been made regarding the contributory factors for the remarkable activity of Au particles. Firstly, the very fact of the nanoscale size of the particles will lead to an increased proportion of the available Au atoms being in low co-ordination sites, which would be expected to increase their reactivity.[6] Similarly, many of these low co-ordination sites will be at the interface between the catalyst particle and its support. The oxide supports used in this area are generally classified into reducible, those for which it is possible to affect the metal ion oxidation state by changing the oxygen chemical potential of the environment (TiO_2, Fe_2O_3 *etc.*) and non-reducible, those in which the metal ion oxidation state is fixed for all accessible reaction conditions (MgO, Al_2O_3 *etc.*). It is generally observed that

---

Cardiff Catalysis Institute, School of Chemistry, Cardiff University, Main Building, Park Place, Cardiff, UK CF10 3AT. E-mail: willockdj@cf.ac.uk

† Part of a thematic issue covering the topic of gold: chemistry, materials and catalysis.

Dr Rudy Coquet graduated from ISMANS in France (http://www.ismans.fr/international/) with an MSc in materials science. As his final year internship in 2002 he went to the Mitsubishi Chemical Corporation at their main research centre in Yokohama, where his interest in molecular modelling of catalysts began. His PhD in Cardiff was funded by SASOL working on oxidation catalysis including supported Au catalysts. In 2005 he took up a postdoctoral position with Prof. Yasuhiro Iwasawa at the University of Tokyo, funded by the Japanese Society for the Promotion of Science (JSPS). In 2007 he moved to the Nippon Oil Corporation in Yokohama, as a senior chemist and is now a member of the Fuel Research Laboratory in the Research & Development Division where he runs the research molecular modelling group.

Kara Howard graduated from the University of Southampton in 2005. During her degree she worked for six months in Richard Keene's group at James Cook University, Townsville, on the design of metallosupramolecular host molecules for recognition of chiral anionic guests. In 2006 she obtained an MSc in molecular modelling from Cardiff University, and is currently working toward a PhD under the supervision of Dr David J. Willock using DFT to simulate the structure and reactivity of gold nanoparticles on oxide supports.

Dr David J. Willock gained his PhD at Queen Mary College, London and then carried out postdoctoral work at UCL and the Royal Institution on the simulation of organic crystal structures working with Prof. S. L. Price and Prof. C. R. A. Catlow. He moved from London to the Leverhulme Centre for Innovative Catalysis, Liverpool University in 1993 and has worked in the area of computer simulation applied to catalysis ever since. In 1997 he became a lecturer in the School of Chemistry, Cardiff University where he now works on the application of periodic DFT to adsorption and reaction of molecules on surfaces. He also actively develops atomistic codes, including Monte Carlo methods for template design which have been used to generate new catalytic materials.

supports formed from reducible oxides lead to catalysts that are more active than those using non-reducible support materials, reinforcing the idea that the perimeter region of the Au particles may be important. It has also been suggested that, for the reducible oxides at least, the oxidising species is supplied from molecular oxygen adsorbed on the surface of the support, rather than directly from gas phase O_2 interacting with the Au particle surface.[7] Another influence of the support could be to strain the lattice of the Au particles adsorbed upon it.[8] If the interaction of the support and the oxide requires a degree of epitaxy between the metal and underlying oxide lattice the former will tend to be strained, with the resulting decrease in binding energy for the particle being compensated by the interfacial energy. Again, this would be expected to weaken Au–Au bonds and so make the Au atoms more likely to become involved in the reactions with adsorbates.

The response of low co-ordination atoms to adsorbates may also be important through dynamic structural fluxionality. This implies that the restructuring of the particles in response to the presence of the reactants may lower the barrier to reaction. These effects are also likely to be more significant for smaller particles since the planar facets of larger clusters contain Au atoms that have more Au–Au interactions to restrain them.

Interactions of an electronic nature between the metal particles and support will also occur. The most important of these is charge transfer from the support to the particles, particularly for particles adsorbed at defect sites. For small Au clusters this effect is likely to be more significant since the transferred charge cannot be as widely distributed as in larger particles. In addition, for very small particles the electronic structure will be closer to the discrete molecular orbital picture rather then the continuous band like states of macroscopic metal particles; influencing their behaviour through electronic size effects.

Norskov and co-workers[9,10] have compared experimental data for both reducible and irreducible supports to point out that the most important experimental parameter, by far, is particle size. Irrespective of the support used, CO activity becomes significant for catalysts containing average particle diameters of between 2 and 5 nm. To put this into context for modelling studies it is informative to estimate the number of atoms it represents. Metallic Au in the bulk phase has an fcc unit cell with a lattice constant of 4.08 Å. This means a volume per atom of 17 $Å^3$ and so, if we assume a hemi-spherical shape, these average nanoparticles contain 125–1900 Au atoms. In modelling terms, particles on this scale are still quite large, because density functional theory (DFT) methods for atoms as heavy as Au are still restricted to a few 10s of atoms for anything other than showcase calculations. However, clusters with computationally accessible dimensions are still of interest since they may contain all the features required for catalytic activity. Indeed, there is experimental evidence that much smaller Au clusters can be active for CO oxidation. Landman and co-workers have studied size selected metal particles deposited with low kinetic energy onto MgO thin films, and estimate that significant CO oxidation activity is detected for clusters as small as Au_8.[11]

The majority of simulation studies have concentrated on models that address one or more of the above aspects of Au catalysis. This review will attempt to bring together data from calculations on isolated Au clusters, periodic work on Au surfaces and the interactions of Au particles with oxide surfaces. The overall aim is to summarise current thinking on the important aspects of the CO oxidation reaction including the adsorption of the reactants, their interaction to form CO_2 and the possible roles played by water.

For the smaller particles, molecular simulation codes have been used to study the properties of Au clusters without explicit representation of the support. This isolates the effects due to particle size and shape without the complication of the support interface, giving insight into the features that are responsible for the intrinsic reactivity of Au particles. At the other extreme, calculations using periodic DFT have considered high Miller index surfaces of bulk gold. These models contain low co-ordination sites at steps and kinks in the metal surface, but clearly have the band structure fully developed in contrast to the discrete orbitals of the molecular cluster approach.

Some of these aspects have been covered in a recent short review of the mechanistic insights available from DFT calculations.[12] In this contribution we will attempt to broaden the discussion to include the reliability of the calculations currently in the literature. The workhorse for all these calculations has been DFT in its various guises. For small clusters the more accurate coupled cluster approach has been used to generate reference data and this, along with comparison to experimental data, will be used to assess the reliability of DFT in this area. This leads into a discussion of the preferred structures and the electronic characteristics of Au particles in isolation. The effect of particle shape and charge on the adsorption of CO and O_2 will be summarised along with the reaction pathways that have been put forward based only on calculations with effectively gas phase Au clusters. Finally, we will cover the introduction of a support material, usually using MgO as a model non-reducible oxide or TiO_2 as a reducible one. A great deal of work has been invested in describing the metal/oxide interface and exploring the role of oxide defect sites in anchoring the metal particles. The ultimate goal is to follow the actual oxidation of CO with the model of the support in place and the attempts to do this will be summarised.

We start with a brief overview of the theoretical concepts that need be considered in any simulation involving Au, of which relativity is central.

2. Atomic properties of Au, relativistic effects and computational approaches

Gold is a late transition metal belonging to group 11 of the periodic table along with Cu and Ag, it has a doublet ^2S ([Xe] $6s^1 4f^{14} 5d^{10}$) atomic ground state. With an atomic mass of 196.97 amu the electronic energy levels of Au are strongly influenced by relativistic effects. The theory of the electronic structure of Au, and other heavy elements for which relativity has a qualitative effect, have been the subject of several reviews, most notably by Pyykkö.[13–15] The fast moving electrons that are directly affected are in the low lying core states of the atom which experience the unshielded potential of the nucleus. For example, 1s electrons move with classical speeds in atomic units (au) roughly equal to the nuclear charge, Z.[16] The speed of light (c) is 137.036 au and so the 1s electrons of Au move at around $0.58c$. As a consequence the electrons occupying Au(1*s*) are 1.51 times more massive than when at rest, since relativity introduces a velocity dependent mass. In addition, relativity leads to a stronger coupling between each electron's spin and orbital angular momentum than would be found for lighter elements. This means that *j–j* rather than Russell Saunders' coupling would be used to describe multi-electron term states.

A full treatment of these effects requires solution of the four component Dirac equation,[17] but this is extremely difficult, both in the effort of encoding the mathematics and the time required to run calculations. At the present time calculations are limited to generating reference data on single atom or diatom systems.[18] To make progress techniques for transforming to a two component formulation have been introduced. For example the Pauli equation, which can be written,

$$\left[\frac{p^2}{2m}+V-\frac{p^4}{8m^3c^2}+\frac{Z\vec{s}.\vec{l}}{2m^2c^2r^3}+\frac{Z\pi\delta(r)}{2m^2c^2}\right]\psi_{\mathrm{L}}=E\psi_{\mathrm{L}} \qquad (1)$$

where p is the momentum, m the rest mass and r the position of the electron. The wavefunction is split into large, ψ_{L} and small, ψ_{S}, components, but the essential physics is contained in this expression for ψ_{L} alone.

The first two terms in eqn (1) are the kinetic energy and the potential due to any external fields, such as the nuclei of a molecule. These are the same as in the more familiar Schrödinger equation, to which the Pauli equation reduces when the electron velocity is much less than the speed of light (p and Z small). The remaining three terms in the square bracket describe the effects of relativity. The first of these is the mass-velocity correction which takes account of the link between the electron mass and its speed. The second term containing a speed of light dependence describes spin orbit coupling through a vector dot product of the electron spin and orbital angular momentum, $\vec{s}\cdot\vec{l}$, while the final term in the Hamiltonian is the Darwin correction. Unlike the spin–orbit term, the mass–velocity and Darwin terms do not depend on vector quantities. Approximations taking only these two terms into account are accordingly referred to as scalar–relativistic (SR) methods.

An alternative approach to the Pauli equation that gives a one-electron relativisitic Hamiltonian for use in density functional theory has been developed by Baerends and co-workers.[19] They write a density functional version of the Dirac equation and then use a truncated mathematical expansion of the relativistic contributions to the energy.[20] This gives the zero order regular approximation (ZORA) which does include spin–orbit terms. All electron calculations using the ZORA approach can be compared to scalar relativistic results to estimate the importance of spin–orbit coupling.

The dependence of electron mass on velocity leads to the well known core contraction for the heavy elements which must be reproduced in any realistic computer simulation. Although the inner core region will be the most strongly affected, the atomic orbitals more remote from the nucleus still have wavefunctions that venture, with some probability, into the core region. These must remain orthogonal to the core states, and so a shift in the core nodal patterns also leads to contraction for the higher *ns*-states. For elements in the same mass range as Au the effect is felt right out to the 6s orbital. One advantage of computational chemistry is that terms in the Hamiltonian can be switched on and off at will and so a direct comparison of non-relativistic and relativistic calculations can be made to quantify these effects. Fig. 1 shows the relativistic contraction of the 6s shell for elements Cs (Z = 55) to Fm (Z = 100) taken from Pyykkö's early review.[13] The contraction is almost 20% for Au, which is also the maximum seen for the stable elements. Following the same orthogonality argument, the outer *p*-states also contract but *d* and *f* level orbitals expand away from the nucleus. For the valence states of gold the contraction gives stabilisation of the 6s level and destabilisation of the 5d levels. This brings them closer together in energy than would be the case in the absence of relativitistic effects and so bonding patterns requiring *sd* hybridisation are enhanced.

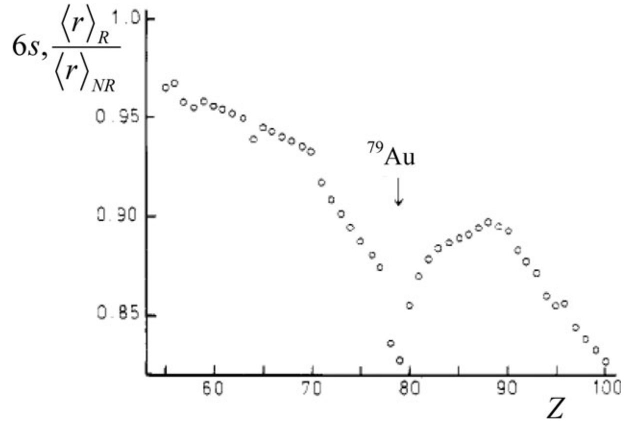

Fig. 1 The core contraction of the 6s orbital for elements Cs to Fm shown as the ratio of the average electron-nuclear distances obtained from a relativistic, $\langle r\rangle_R$, and non-relativistic $\langle r\rangle_{NR}$ calculation. Reprinted with permission from ref. 13. Copyright 1988 American Chemical Society.

The effect of the inclusion of scalar relativistic corrections and fully relativistic (including the spin–orbit term at the ZORA level of approximation) has been studied for the bulk properties of the Group 11 elements by Philipsen and Baerends[21] and the results relevant to bulk Au are summarised in Table 1. At the non-relativistic (NR) level the lattice constant is overestimated by around 9% due to the lack of a core contraction. This also leads to an underestimate of the cohesive energy and bulk modulus. Including scalar relativistic corrections (SR) recovers the lattice constant which is now only overestimated by 2.7%, in line with gradient corrected DFT results for lighter elements. The cohesive energy and bulk

Table 1 Comparison of calculated bulk properties of Au with different levels of relativistic effects taken into account

Property	NR	SR	FR	Expt.
Lattice constant/Å	4.45	4.19	4.17	4.08
Cohesive energy/eV	2.11	2.84	2.99	3.81
Bulk modulus/Mbar	0.71	1.32	1.30	1.73

Note: Results from ref. 21 calculated using GGA corrections (Becke exchange and Perdew correlation) to the LDA density at the NR; non-relativistic, SR; scalar-relativistic and FR; fully relativistic (ZORA) levels.

modulus are correspondingly improved, but the errors are still quite large, almost 1 eV and 0.41 Mbar, respectively. It should be noted that the improvements on including spin–orbit interactions in the Hamiltonian are actually marginal; the major relativistic effects appear to be described at the scalar relativistic level.

Core potentials

We have seen that the SR core contraction mainly requires a description of the core states and their interplay with the chemically important valence electrons. Almost all calculations aimed at understanding catalysis require the inclusion of several Au atoms, adsorbates and possibly the support oxide. It is also necessary to study several different adsorption geometries for each reactant and the comparison of alternative pathways requires many calculations to be undertaken. All electron calculations that deal explicitly with the core states would be computationally expensive, even without the added complication of relativistic effects. For these reasons, almost all the results presented in this review have replaced the core electron states with a potential that mimics their influence on the valence electrons. This allows calculations to deal with the bonding states without expending too much computational effort on the lower energy atomic states. In molecular quantum chemistry, using localised basis functions for the valence states, these potentials are referred to as effective core potentials (ECPs). In calculations using periodic boundary conditions and a plane-wave basis set the term "pseudopotential" is more popular.[22] In addition to the greater computational speed that these potentials allow, the main relativistic effect of the core contraction can also be included by adjustment of the core potential. This means that the reference calculations that are required to set up the pseudopotential should explicitly include relativity, but the everyday application to a chemical problem can be carried out using the more widely available non-relativistic approaches, since the valence state electrons have much lower kinetic energies. The potential replacing the core states should represent the core contraction caused by the scalar relativistic effects and its influence on the valence electrons.

The parameterisation of an ECP is usually carried out using computationally expensive all-electron calculations for reference data by groups specialising in electronic structure methods. The aim is to produce a consistent set of potentials and basis sets to cover a broad range of elements. In molecular quantum chemistry codes such as Gaussian03[23] the established ECPs of Hay and Wadt along with the associated basis functions have been included as a standard part of the basis set library. There are two variants both fitted to scalar-relativistic calculations on atoms and published in 1985. The first, a "large" core potential replaces the standard [Xe] core and the 4f levels and is used along with a basis covering 5d, 6s and 6p orbitals.[24] This literal interpretation of the "core levels" can lead to problems when states that are formally part of the core have an influence on bonding. For example in describing cationic Au the outermost core states, 5s and 5p levels, may become important in an accurate description of bonding. The second Hay and Wadt potential copes with this by explicitly including these levels in the basis and using a "small" core potential.[25] Although slightly more computationally expensive, the advantages in accuracy have meant that this has become the default option and is commonly referred to as LANL2DZ in the literature. The DZ part of this shorthand indicates that the basis set employed for the valence region is of double zeta type.

Effective core potentials are continually under development to improve their performance. This is partly driven by the availability of more accurate implementations of the Dirac equation for the reference atomic state calculations. For example the group of Stoll have recently developed a series of ECPs for Au and other heavy elements[26] along with complimentary valence state basis sets.[27] The ECPs of Stevens *et al.*,[28] for which we use the acronym SBKJC, have also been used in some of the cluster work discussed later.

For periodic calculations the use of a plane wave basis set to represent the electronic core regions of the valence states can be computationally expensive. The wave functions generated in all electron calculations without pseudopotentials contain radial oscillations near to the atom centres which require a large number of plane waves to reproduce correctly. For this reason, along with the pseudopotentials, pseudo-wavefunctions are introduced. An example from our own work to generate an Au pseudopotential[29] is shown in Fig. 2. A comparison of the all electron and pseudo-wavefunction radial behaviour shows that they are identical outside a cut-off, r_c, where the bonding interactions for valence electrons will occur. Inside r_c the characteristic oscillations can be seen for the all electron wavefunction but these are removed in the pseudo-wavefunction. This pseudopotential/wavefunction was generated following the methodology of Troullier-Martins[30,31] (TM) which gives a norm-conserving pseudopotential, meaning that the fractional population of an electron represented by the real and pseudo-wavefunctions is the same. This restriction is sometimes lifted to give good performance with even smaller plane-wave basis sets. A popular approach is the ultrasoft pseudopotential (USPP) idea introduced by Vanderbilt.[32] More recently a further alternative for representing the core states using the projector augmented waves (PAW) has been introduced.[33,34] In this approach the core states are

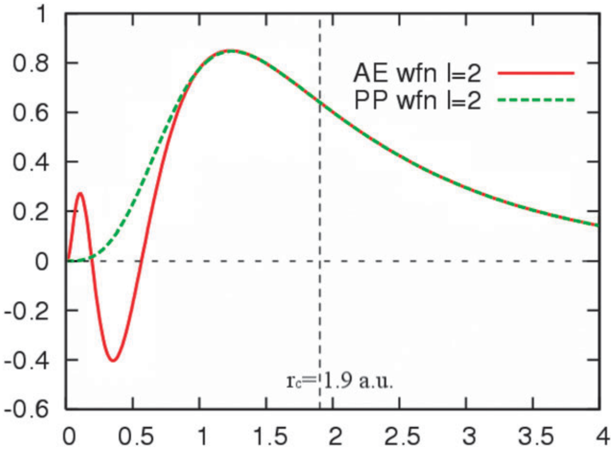

Fig. 2 All-electrons (AE) and pseudopotential (PP) wave functions for gold atomic orbitals with $l = 2$ angular quantum number, r_c is the radius cutoff in au (1 au = 0.5291772 Å). From ref. 29 – Reproduced by permission of The Royal Society of Chemistry.

represented by the potential of a set of core orbitals so that the core electrons appear to be present, but do not enter the variational optimisation of the electronic structure.

DFT functionals, other methods

The speed of DFT comes about from its one electron approach; the Kohn–Sham equation treats each electron as moving in the potential of the nuclei, or pseudopotential representations of atomic cores. The electrostatic field of the other electrons and an effective potential which represents exchange and correlation are taken from the electron density of the system which is also used to estimate the electron kinetic energy. Almost all the pure DFT results presented here also use the gradient of the density to estimate the exchange and correlation potential, in the generalised gradient approximation (GGA). The form of the potential is based on accurate uniform gas calculations and there are many different approaches to the parameterisation of this data to give a GGA. These are given acronyms based on the names of the people who developed them. Among the most widely used are PW91 (Perdew and Wang 1991)[35,36] and BLYP (the exchange functional of Becke[37] with correlation functional from by Lee, Yang and Parr[38]), BPW91 (Becke exchange with PW91 correlation), PBE (Perdew, Burke and Ernzerhof)[39] and its revision RPBE.[40] The revised PBE functional has been shown to improve the description of adsorbates on metals.[41]

One limitation of the GGA approach is that each electron contributes to the density from which its own potential is derived. This gives rise to the self interaction problem, which tends to favour de-localised solutions of the Kohn–Sham equation and give underestimates of the band gaps of insulating materials. One approach to improving the accuracy of these methods is to add in some of the exact exchange available in the Hartree–Fock electronic structure method. This leads to hybrid functions such as B3LYP[42] for which the amount of exact exchange was optimised with reference to molecular data. In the solid state the amount of exchange affects properties such as the calculated band gap. For example Zhang *et al.*[43] have shown that for TiO_2 the calculated band gap increases in proportion to the amount of exact exchange included in the functional. The optimal choice of 13% exact exchange gives a perfect match to the band gap energy. The choice made in B3LYP is slightly larger at 20% but the well documented performance of this functional for molecular bond energies makes it a good compromise for giving reliable properties of the solid and adsorbates when modelling catalytic reactions. Further tailoring of the amount of HF exchange to use according to the solid state property of interest has been discussed by Cora *et al.*, who also show that the introduction of HF exchange increases electronic localisation.[44]

The use of a potential for the correlation part of the electron energy in DFT and hybrid DFT also means that only the static correlation is represented and the dynamic correlation, required to describe the van der Waals dispersion interaction, is omitted. Dynamic correlation can be calculated with post-Hartree Fock methods of which the coupled cluster with singles, doubles and pertubative triples (CCSD(T)) is the most accurate method that has been applied to Au cluster calculations. These methods also have the advantage of giving a more satisfactory account of open shell systems. The spin of the system is a property of the wavefunction, rather than the density, and so is poorly described by DFT. This becomes particularly apparent when alternative spin states are close in energy. For example, for a metal cluster the singlet and triplet solutions may be only a few meV apart. Spin unrestricted DFT will give an energy for each spin setting but these are not pure spin states. On the other hand CCSD(T) will give a weighted mixture of the Slater determinants for the singlet and triplet solutions.

However, the scaling with electron number (N_e) is poor in CCSD(T), with computer time proportional to N_e^7. This limits its application to a few reference calculations on small clusters that we will mention to gauge the accuracy of DFT.

3. Structure and electronic properties of Au clusters in isolation

Small clusters of Au have been extensively studied to discern the factors controlling their preferred shape from their electronic structure. The smallest cluster with some geometrical isomers is Au_3. An M_3 triangular cluster with equivalent bonds will have the point group D_{3h}. Fig. 3 shows that, if we just consider the molecular energy levels formed from linear combinations of the outer most 6s atomic orbitals, the highest occupied molecular orbital (HOMO) is one of a degenerate, e', pair of states. This gives rise to a classic Jahn–Teller distortion in which the energy of the occupied state is lowered by a geometric distortion to C_{2v}. This effect was noted in the early CASSCF calculations of Balasubramanian and Liao[45] who found the lowest energy structure to be an isosceles triangle with an apex angle of 54° (shortened base) with a barrier to the linear $D_{\infty h}$ structure.

In the calculated structures shown in Fig. 3 the preferred distortion is an isosceles triangle with an elongated base. This gives a lower anti-bonding character for the b_1 orbital than the

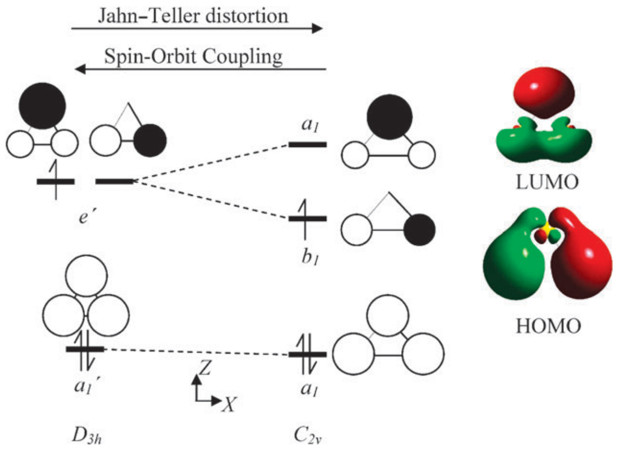

Fig. 3 The Jahn–Teller distortion for the Au_3 complex. The molecular orbitals shown to the right were generated using the B3LYP functional with a Stuttgart effective core potential[26] and associated valence double zeta basis set.[27]

equivalent member of the D_{3h},e' pair. The energy of its unoccupied partner, which now has a_1 symmetry, is raised due to anti-bonding character along the two equivalent sides of the triangle which have been shortened. This distortion is not seen for members of the preceding group, *e.g.* Pt_3 clusters remain as equilateral triangles since the e' level is unoccupied. Similarly Au_3^+ has a calculated stable D_{3h} structure.[46]

In a recent survey of cluster geometries using PW91 with scalar relativistic PAW core states Xiao *et al.*[47] find that the alternative short and long base isosceles triangles that can result from Jahn–Teller distortions are practically degenerate. The C_{2v} structures are also only around 0.05 eV lower in energy than the D_{3h} case. However the lowest energy structure found for Au_3 has an apex angle of 137°. The three minima identified are within 0.1 eV and the highest barrier to their inter-conversion is only 0.13 eV. The long base triangle structure has also been inferred from EPR experiments of Au_3 in a benzene matrix.[48]

There are also reports that the inclusion of spin–orbit coupling in all electron calculations on Au_3 stabilises the D_{3h} geometry which compares well with Au_3 vibrational spectra at 3.5 K.[49] This effect is ignored in calculations using scalar relativistic pseudopotentials. However, the small energy differences between the alternative geometries suggest that, at the temperatures relevant to catalysis, the structure will be quite dynamic, with particles rapidly moving between the alternative symmetries due to thermal excitations.

For even-numbered clusters the outer MOs formed from the 6s atomic orbitals will contain an even number of electrons and so be less prone to symmetry induced distortions. This difference in electronic structure is also reflected in some of the cluster properties. For example the electron affinity shows odd/even oscillations with the number of Au atoms. Maxima are found for the odd clusters n = 1, 3, 5, both experimentally[50] and through DFT calculations.[51]

The geometric diversity available increases rapidly with cluster size, broadly giving linear, zig-zag, planar (2D) and 3D alternatives. For clusters up to Au_{13} Xiao *et al.*[47] find that the highest binding energies (most stable clusters) are for 2D geometries with 3D taking over only for Au_{14} and above, as shown in Fig. 4. This preference for 2D over 3D structures is a consequence of the relativistic effects on the 6s and 5d orbital energies. Relativity brings these closer together which favors the sd hybrid orbitals responsible for bonding in the plane. Linear and zig-zag forms are only competitive up to around Au_5 after which the gap between these and the 3D alternatives increases rapidly to 0.3 eV and above. The differences between the 2D and 3D forms for cluster sizes from Au_7 are less than 0.1 eV.

The switchover between planar and 3D structures using explicitly correlated methods actually occurs earlier than that predicted by DFT. At the CCSD(T) level Gordon and co-workers[52] find that the Au_6 cluster has a preferred planar structure in agreement with B3LYP. However, Au_8 gives a 3D structure with T_d symmetry that is 0.21 eV lower in energy than the planar structure suggested by B3LYP. The B3LYP calculations put this T_d cluster 0.65 eV higher than the lowest energy D_{2h} planar structure. In the breakdown of contributions to the energy it is pointed out that the triple excitation terms of the CCSD(T) calculation give a stabilisation of 0.34 eV and so are crucial to the comparison of the relative stability of the alternative cluster geometries. This suggests that dispersion interactions play an important role in determining the cluster geometries. The T_d cluster has a greater number of short range Au···Au interactions than does the D_{2h} alternative and so is stabilised by the van der Waals dispersion force. DFT calculations do not include the dynamic correlation effects required to capture this part of the system energy.

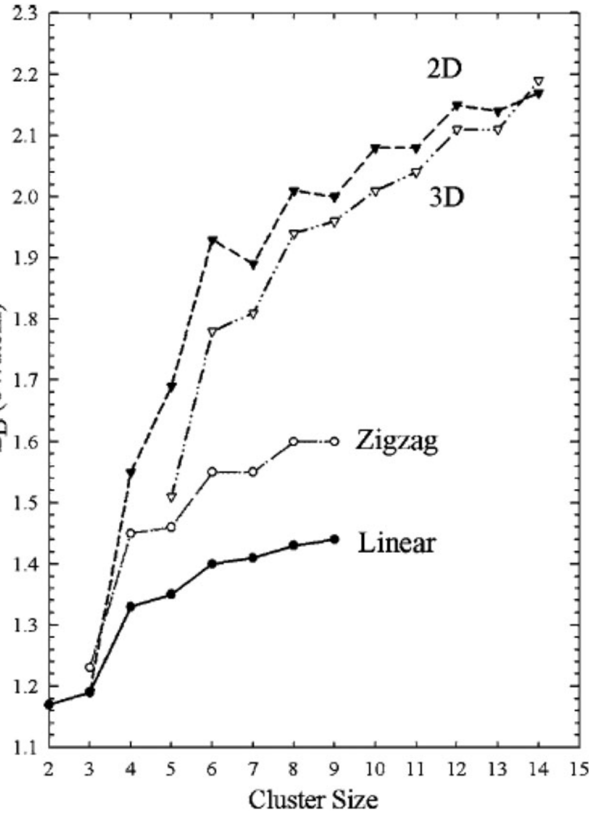

Fig. 4 The binding energies of alternative structure classes for Au_n clusters as a function of cluster size, n. Reused with permission from ref. 47. Copyright 2006, American Institute of Physics.

Within the four geometry classifications there are also more subtle geometric isomer possibilities. For example, in Xaio's paper there are 7 reported 3-D Au_{10} clusters.[47] Au_{10} is often used as a model catalyst particle in the cubooctahedral form, Au_{10}(7,3) with 7 atoms forming an hexagonal close packed layer and the other 3 occupying alternate hollow sites to form the second layer as shown in Fig. 5. This shape is easily cut from the fcc bulk structure and has the facets observed from electron microscopy of larger particles deposited on TiO_2(110) which show Au(111) aligned with the oxide interface.[53] From Xaio's calculations the Au_{10}(7,3) geometry is actually one of the least stable alternatives, however the energy range of all 7 structures is only 0.07 eV and Au_{10}(7,3) has a binding energy just 0.14 eV lower than the most stable planar structure.

In most of these discussions of the preferred geometries of small Au clusters the alternative minima are within a few tenths of an eV of each other and seem to be separated by relatively small barriers. This means that on an oxide support the shape of the cluster will be strongly influenced by the interaction of the particles with the surface since the small

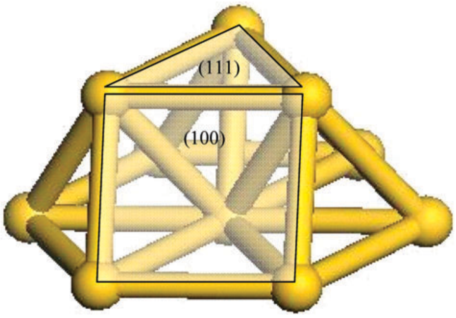

Fig. 5 The Au_{10}(7,3) cluster with planes indicating example faces with the geometry of Au(111) and Au(100) bulk planes.

energy differences in the intrinsic relative stability of clusters may be overridden by the interfacial energy.

The importance of the interfacial energy on the cluster geometry has been recognised by many workers simulating the adsorption properties of these particles. Some prefer to use clusters which are the optimum geometry for that number of Au atoms in the gas phase. Others take the view that the cluster will in some way be constrained geometrically by interaction with the support material. To account for this, the atoms in the cluster are constrained. For example, the Au_{10}(7,3) cluster used by Nørskov and co-workers has the constraint that the lower 7 atoms are must have the same z-coordinate.[54]

Cluster size and shape also influences the electronic structure of Au particles. It would be expected that as the cluster size is increased the orbital description of the molecular approach would give way to a band picture of electronic states. In particular in the band structure for bulk Au, illustrated in Fig. 6, the Fermi level is in the sp part of the valence band with a negligible gap between occupied and unoccupied states.

As we have seen in the Au_3 example, cluster calculations give distinct molecular orbitals with a gap between the occupied and unoccupied states. This gap should narrow as the cluster size increases, and vanish as the metallic bulk is approached. Fig. 7 shows the calculated HOMO–LUMO gap for Au_n (n = 5–14) from the cluster calculations of Xiao *et al.*[47] using the hybrid functional B3LYP. It is known from the solid state simulation literature that this hybrid functional gives a better account of the gap between valence and conduction bands in semi-conductors and insulators than does the GGA approach, which always underestimates E_G.[55] In the cluster calculations there is a decrease in the average energy gap for cluster sizes above Au_8, but significant values of E_G, averaging around 0.75 eV, are still apparent for the larger clusters. Additional calculations on Au_{55} gave HOMO–LUMO gaps of 0.69 and 0.29 eV for the two geometries considered. It appears, then, that the electronic structure of the small clusters used in most simulations of Au catalysis are best thought of as being described by a discrete set of molecular orbitals with a significant HOMO–LUMO gap. The band structure description is only appropriate for the very largest clusters. However, STM measurements have suggested that the metal/non-metal switch over point for Au particles supported on TiO_2(110) occurs somewhere around particles of height 0.4 nm.[56] For a hemispherical particle this will correspond to roughly Au_8, and so these significant E_G estimates for considerably larger particles may be due to the omission of the support in the calculations.

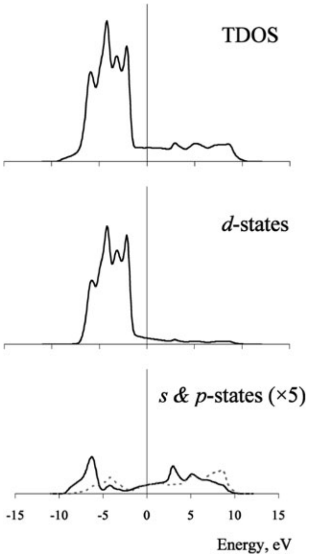

Fig. 6 The calculated density of states for optimised bulk Au. Calculation used the PBE functional, a plane wave basis and PAW representation of core states, k-point sampling employed 455 unique points. Top: total density of states (TDOS), middle and bottom: partial density of states (PDOS) for d and s (solid line) & p (dotted line) contributions. The tail on the PDOS for Au(d) orbitals is due to the projection onto the PAW orbital basis not being exact.

In summary, calculations on isolated Au clusters point to planar structures for the smallest particles, up to around Au_{13} according to DFT, after which 3D forms have a lower overall energy. This encompasses most of the simulation work presented in this review on supported clusters and certainly includes particles that are thought to be active for CO oxidation from surface science experiments. The small difference in the energies of alterative cluster geometries suggests that the actual structure

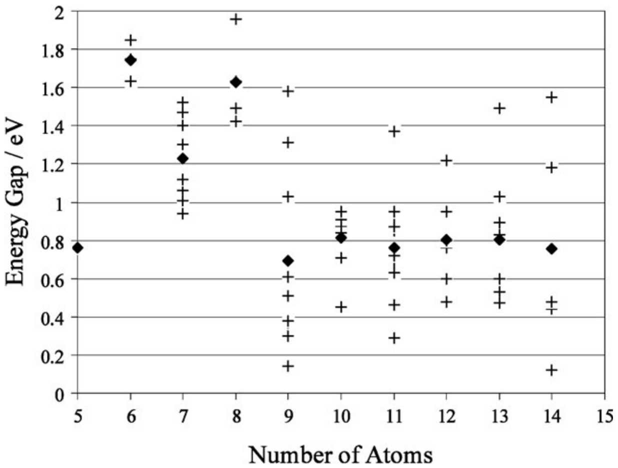

Fig. 7 Energy gap as a function of cluster size for Au_n at the B3LYP level for the 3-D clusters of ref. 47. The multiple points (+) for each value of n are for different cluster geometries, average values are marked with solid diamonds.

of Au catalyst particles will be influenced by interaction with the oxide support and the adsorption of reactant gases.

Larger clusters have also been considered at the gradient corrected DFT level. Rösch and co-workers[57] considered the convergence of the properties of 3D clusters from Au_6 to Au_{147} based on clusters with O_h and I_h symmetries. While Barnard and Curtiss[58] identify the preferred point group symmetry of clusters containing "magic" numbers of Au atoms from 19 to 146.

4. The CO reaction potential energy surface on Au surfaces and clusters

The energetics of possible CO oxidation reaction profiles without explicit inclusion of a support material have been reported by a number of workers. Two approaches will be covered in this section, the use of a periodic simulation of the surfaces of bulk Au and the use of clusters to represent smaller particles. Some of the support effects discussed in the Introduction section have also been introduced indirectly, using constraints on atom positions in a cluster to mimic the interface with the oxide, for example. For the periodic simulations the effect of strain induced by the particle/support interaction can be introduced by adjusting the surface vectors of the simulation cell. For cluster calculations charging of the catalyst particles by charge donation from the surface is represented by giving the simulated system an overall negative charge. The reduced electron density implied by partial oxidation of the cluster can be represented by adding an overall positive charge. This has the advantage that the exact identity of the oxidizing species need not be considered. When only the Au component of the catalyst is included in a simulation the adsorption of both CO and O_2 on the metal surface must be considered prior to any reaction steps.

CO adsorption

For CO the usual model of bonding to a transition metal centre involves donation from the 5σ orbital ($M \leftarrow CO$) accompanied by back donation from the metal d-orbitals to the empty anti-bonding 2π molecular orbital, ($M \rightarrow CO$). The weakening of the CO bond by the back donation generally leads to lengthening of the CO bond accompanied by a red-shift in the observed CO stretching frequency compared to gas phase CO. In Au the 5d orbitals are filled and, despite the scalar relativistic core contraction, are below the singly-occupied 6s state. This means that their involvement in the Au–CO bond is likely to be weak, indeed it has been suggested that the covalent component of Au–CO bonds in complexes is quite low. The major part of the interaction being electrostatic, involving the small $(-)C{=}O(+)$ dipole which is enhanced through interaction with a cationic Au centre.[59] The electrostatic interaction increases the bond polarisation of the CO molecule, tending to strengthen the C=O bond and leading to blue-shift in the stretching frequency.

Table 2 gives an overview of calculations on the Au cluster/CO system. The adsorption energy, E_{ads}, values are calculated using the expression,

$$E_{ads} = -E(Au_n\cdots CO) + E(Au_n) + E(CO) \qquad (2)$$

where $E(Au_n\cdots CO)$ is the calculated energy for the Au_n cluster with CO adsorbed and $E(Au_n)$ and $E(CO)$ are the calculated energy for the isolated Au_n cluster and CO molecule, respectively. This definition gives the energy required to remove the CO molecule from the cluster and so positive values correspond to favorable adsorption energies. When a molecule adsorbs to a particle both the cluster and molecular structures will be altered, so the energies for the reference states in (2) should be for the cluster and molecule relaxed in isolation at the same level of theory (functional, basis set and convergence criteria) as the $Au_n\cdots CO$ system. In addition, for calculations using a localised basis set, the basis used in the $Au_n\cdots CO$ calculation will naturally contain more functions than used for either of the reference systems, Au_n and CO. Some of the apparent stabilisation of the $Au_n\cdots CO$ structure will arise from its richer basis set, an effect referred to as basis set superposition error (BSSE). This can be corrected for by including all the basis functions of the $Au_n\cdots CO$ system in the reference calculations.[60] Where available, Table 2 quotes the BSSE corrected values. For plane wave basis sets BSSE will not occur since the size of the basis set is determined by the energy cut off used to control the number of plane waves in the simulation. Provided the same energy cut off is used in all three calculations required for eqn (2), the basis set levels will be consistent.

To describe the geometry of the adsorbed states we have used the nomenclature commonly applied to metal co-ordination complexes. An η^m co-ordination has the adsorbed molecule at a single metal site with m atoms of the adsorbate in contact with the metal atom. A μ_n co-ordination involves bridging of an adsorbate molecule between n metal atoms. Adsorption of CO to Au clusters is exclusively *via* the C atom.

Au_1 anions or neutral species adsorb CO relatively weakly.[61] The B3LYP results show negligible binding for the anion and a low value of only 20–30 kJ mol^{-1} for the neutral atom. The PW91 values appear more favorable by 40–50 kJ mol^{-1}, but as will become clear, this is probably due to a systematic tendency of this functional to overbind. The high binding energies with PW91 are accompanied by large red shifts in the calculated CO stretching frequencies, suggesting that this functional overestimates the metal–ligand back donation into the CO 2π* anti-bonding orbital. The PW91 structures have a non-linear Au–C=O angle, so that back donation can occur from orbitals with σ-symmetry with respect to the Au–C bond. In the linear B3LYP structures back donation requires π-symmetry overlap between Au and C=O orbitals. The calculated frequencies at the B3LYP level are found to give good agreement with measurements made on matrix isolated complexes from laser ablated Au atoms.[62]

For Au_2 a similar pattern is seen, although now CO is bound more strongly than in Au_1 in the anionic and neutral complexes, while the binding to Au^{2+} is actually slightly weaker (comparing PW91 results) than for Au^+. The PBE results here appear to show stronger binding than the PW91 functional, along with a smaller red shift in the vibrational frequencies. However this comparison may also be influenced by the use of different basis sets in the calculations. The structure calculated by Häkkinen and Landman[63] for the $[Au_2–CO]^-$ is shown in Fig. 8a showing the characteristic "bent" geometry of Au–C=O. Some papers show illustrations

Table 2 Summary of calculated data for CO adsorption to isolated Au_n clusters

Cluster	Method[a]	$E_{ads}(CO)$/kJ mol^{-1}	Co-ord., Au C.N. [Au geom.][b]	Au···C═O, θ/degrees	CO freq./cm^{-1}	Ref.
Au^-	PW91/L2DZ(Au)/6-311G(d)(C,O)	44	η^1, 0	$90 < \theta < 180$	1860	46
	B3LYP/L2DZ(Au)/L2DZ + pd(C,O)	1	η^1, 0	180	—	61
Au	PW91/L2DZ(Au)/6-311G(d)(C,O)	77	η^1, 0	$90 < \theta < 180$	1990	46
	B3LYP/L2DZ(Au)/L2DZ + pd(C,O)	20	η^1, 0	180	—	61
Au^+	PW91/L2DZ(Au)/6-311G(d) (C,O)	248	η^1, 0	180	2228	46
	B3LYP/L2DZ(Au)/L2DZ + pd(C,O)	195	η^1, 0	180	—	61
Au_2^-	PBE/TM PPs/plane wave	93	η^1, 1	132	1841	62
	PW91/L2DZ(Au)/6-311G(d)(C,O)	75	η^1, 1	$90 < \theta < 180$	1811	46
Au_2	PBE/TM PPs/plane wave	154	η^1, 1	—	2147	62
	PW91/L2DZ(Au)/6-311G(d)(C,O)	148	η^1, 1	180	2111	46
Au_2^+	PW91/L2DZ(Au)/6-311G(d)(C,O)	195	η^1, 1	180	2199	46
Au_3^-	PW91/L2DZ(Au)/6-311G(d)(C,O)	73	η^1, 1 [lin.]	—	1941	46
	PW91/STO TZP	93	η^1, 1 [lin.]	$90 < \theta < 180$	—	64
		171	η^1, 2 [2D]	180	—	
Au_3	PW91/L2DZ(Au)/6-311G(d)(C,O)	156	η^1, 2 [2D]	180	2088	46
Au_3^+	PW91/L2DZ(Au)/6-311G(d)(C,O)	175	η^1, 2 [2D]	180	2181	46
Au_4^-	PW91/L2DZ(Au)/6-311G(d)(C,O)	92	η^1, 2 [2D]	$90 < \theta < 180$	1949	46
		83	η^1, 1 [lin.]	$90 < \theta < 180$	—	
	PW91/STO TZP	117	η^1, 2 [2D]	$90 < \theta < 180$	—	64
Au_4	PW91/L2DZ(Au)/6-311G(d)(C,O)	154	η^1, 2 [2D]	180	2109	46
		153	η^1, 3 [2D]	180	—	
Au_4^+	PW91/L2DZ(Au)/6-311G(d)(C,O)	154	η^1, 3 [2D]	180	2164	46
		145	η^1, 2 [2D]	180	—	
Au_5^-	PW91/L2DZ(Au)/6-311G(d)(C,O)	115	η^1, 2 [2D]	180	2041	46
		84	η^1, 2 [2D]	$90 < \theta < 180$	—	
	PW91/STO TZP	95	η^1, 2 [2D]	$90 < \theta < 180$	—	64
Au_5	PW91/ L2DZ(Au)/6-311G(d)(C,O)	105	η^1, 3 [2D]	180	2084	46
		96	η^1, 2 [2D]	180	—	
	PBE/TM/DZP(Au)/DZP(O)	122	μ_2, 3,3 [2D]	—	1727	80
Au_5^+	PW91/L2DZ(Au)/6-311G(d)(C,O)	161	η^1, 2 [2D]	180	2163	46
		154	η^1, 2 [2D]	180	—	
Au_6^-	PW91/L2DZ(Au)/6-311G(d)(C,O)	95	η^1, 2 [2D]	180	1967	46
		81	μ_2, 1,2 [2D]	—	—	
Au_6	PW91/L2DZ(Au)/6-311G(d)(C,O)	86	η^1, 2 [2D]	180	2101	46
		57	η^1, 4 [3D]	180	—	
	PBE/TM/DZP(Au)/DZP(O)	93	η^1, 2 [2D]	162	2003	80
Au_6^+	PW91/L2DZ(Au)/6-311G(d)(C,O)	147	η^1, 2 [2D]	180	2166	46
		129	η^1, 4 [2D]	180	—	
Au_7	PBE/TM/DZP(Au)/DZP(O)	124	μ_2, 3,3 [2D]	—	1709	80
Au_8	PBE/TM/DZP(Au)/DZP(O)	111	η^1, 2 [2D]	175	2032	80
Au_9	PBE/TM/DZP(Au)/DZP(O)	103	η^1, 2 [2D]	168	2005	80
Au_{10}	PBE/TM/DZP(Au)/DZP(O)	101	η^1, 3 [2D]	168	2016	80
Au_{12}	PBE/USPP/plane wave	121	μ_2, 6,6 [3D]	—	—	68
Au_{13}	B3LYP/L2DZ(Au)/L2DZ + pd(C,O)	89	η^1, 5 [3D]	180	—	61
Au_{13}^+	B3LYP/L2DZ(Au)/L2DZ + pd(C,O)	90	η^1, 5 [3D]	180	—	61

[a] Method includes functional/Au basis and ECP/O basis and ECP, with L2DZ = LANL2DZ, DZP, TZP = double, triple zeta plus polarisation basis set, STO = Slater type orbitals used without ECPs but with the core states frozen, most other simulations use the standard Gaussian basis as indicated. For pseudopotentials: TM = Troullier-Martins, USPP = ultra soft pseudopotentials, PAW = projector augmented waves. [b] In addition to the co-ordination modes described in the text, μ_2 = end-on CO, bridging 2 Au atoms, Au co-ordination refers to the number of neighbours in the cluster for the co-ordinated Au, for bridging modes two values are given.

of the complexes showing such a structure but do not quote the value of the Au–C═O angle. In Table 2 this is indicated by $90 < \theta < 180°$. Fig. 8b shows the calculated charge density difference between the complex and a reference calculation on non-interacting Au_2^- and CO in the same positions. This illustrates how the charge has re-distributed as the two species interact. The bent geometry allows donation into the C═O $2\pi^*$ anti-bonding orbital from Au_2^- orbitals that have σ symmetry with respect to the Au–C bond. This would not be possible in a linear complex. Fig. 8c gives an alternative μ_2 geometry complex for $[Au_2–CO]^-$, but this has a calculated adsorption energy some 40 kJ mol^{-1} lower than the bent η^1 geometry reported in Table 2.

For Au_3 there is a choice between linear or triangular 2D structures, for the anion binding of CO to the latter is seen to be much more favourable than the former,[64] and comparable with the adsorption energy calculated for the positively charged cluster. Au_4^- anions also show this preference for adsorption to 2D rather than linear structures, although here the adsorption energy difference is only 10 kJ mol^{-1}.

The general trends for the binding of CO to gold clusters as a function of cluster size (n = 1 to 6 in Au_n) and overall charge can be seen from the plot of the data from Wu *et al.*[46] in Fig. 9. The cluster geometries in this study were the lowest energy isomers for each system, these are either linear chains (Au_n^-, n = 3, 4) or planar structures. The lowest adsorption energy found in each

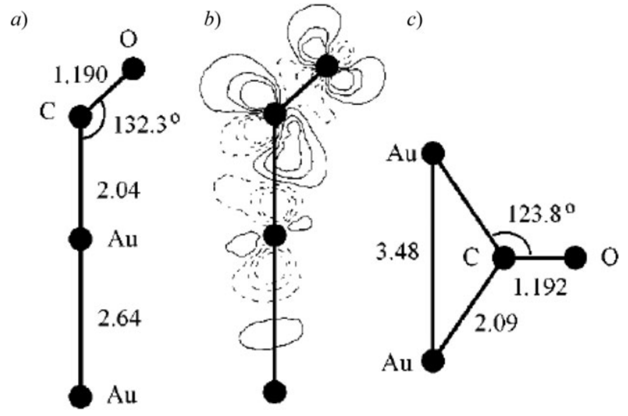

Fig. 8 (a) The structure of $[Au_2CO]^-$ showing the bent Au–C=O geometry. (b) The charge density difference between the final structure and a non-interacting Au^{2-}/CO in the same geometry, the contours of are shown in the range of -0.015–$0.015e$ with $0.006e$ intervals. Dashed (solid) line denotes depletion (accumulation) of the electron density. (c) A bridging CO adsorption geometry. In (a) and (c) bond lengths are in Å. Reprinted with permission from ref. 63. Copyright 2001 American Chemical Society.

case was for CO co-ordinated through a single Au–CO bond. For all cluster sizes considered, the strongest interaction for CO is with the positively charged Au clusters. These show estimated adsorption energies of up to 248 kJ mol^{-1} for $n = 1$ falling to just under 193 kJ mol^{-1} for the larger Au clusters in the series at the PW91 level. The difference between the adsorption energies for the different charge states reduces as the cluster size is increased. For the anionic case this reflects the smaller individual atomic charges that result as the single negative charge placed on the cluster becomes more spread out. For all three graphs the hybrid functional B3LYP gives lower adsorption energies than PW91 by around 39–58 kJ mol^{-1}, but the same trends are seen with either approach.

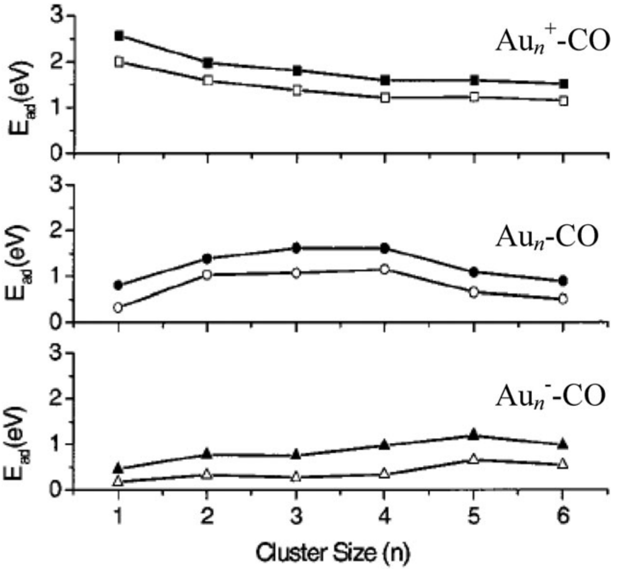

Fig. 9 Calculated binding energies, E_{ad}, for CO adsorbed to Au_n^+, Au_n and Au_n^- as a function of cluster size. Results from PW91 (solid symbols) and B3LYP (open symbols) exchange–correlation functionals are compared. Reused with permission from ref. 46. Copyright 2002, American Institute of Physics.

For the positively charged clusters it is also found that the CO bond length is longer and the calculated frequency higher than for a reference gas phase CO molecule at the same level of theory. While in the anionic complexes the CO bond length is increased and frequency decreased on co-ordination to Au_n^-. While, in principle, the observation for the anionic clusters could arise from increased back donation, it is also in line with the idea that a large component of the M–CO bond comes from an electrostatic interaction.

Most of the structures reported in Table 2 have used the 2D structures predicted to be the most stable forms of free Au up to cluster sizes of Au_{13} (Fig. 4).[47] The co-ordination number of the Au atom acting as the adsorption site is also given in the Table but for these small 2D clusters it seems to have little systematic influence on the calculated adsorption energies. For example, at Au_6, PW91 calculations do show a stronger binding to 2 co-ordinate Au than 4 co-ordinate in the same cluster by 29 kJ mol^{-1}.[46] However, for Au_4 the same reference shows only a 1 kJ mol^{-1} difference between 2 and 3 co-ordinate Au atoms while the variation between atoms of 2 fold co-ordination in Au_5^- is 31 kJ mol^{-1}.

For 3D Au_{13} clusters the difference in adsorption energy for CO on neutral and positively charged clusters negligible.[61] For larger cluster sizes this implies that the single positive charge assigned to the cluster as a whole is too thinly spread to be of influence. The results for negatively charged clusters from Au_5^- show a similar dilution of charge so that greater variation in adsorption energy is seen from choice of adsorption site than as a consequence of negative charging.

Periodic DFT has also been used to study the adsorption of CO to transition metals. The Pt–CO bond has been the subject of a great deal of discussion in this area of simulation. Gradient corrected DFT calculations on the CO/Pt(111) system gives an ordering of the atop and fcc sites which favours the latter by around 24 kJ mol^{-1}.[65] This is contrary to surface science experiments which show CO to prefer atop adsorption.[66] The disagreement is a manifestation of the self interaction effect, an inherent problem of GGA-DFT which gives errors in the treatment of localised charge densities. Such systems can be studied with semi-empirical corrections using the DFT + U approach which has been shown to correctly predict the site preference of CO/Pt(111).[67] As yet this methodology has not been extended to Au surface calculations. However, PBE calculations show that CO binding to Au(111) is much weaker than to Pt(111) at only 16 kJ mol^{-1}.[68] On stepped surfaces the calculated binding energy is much higher due to the availability of low co-ordination Au atoms. The PBE results give 135 kJ mol^{-1} and 96 kJ mol^{-1} for Au(211) and Au(221), respectively. This is much more in line with the common idea that low co-ordination sites are required for CO adsorption than the cluster results discussed earlier. In the Au(111) surface each atom is 9 co-ordinate, while this drops to 7 on a step edge. In the cluster calculations the highest co-ordination numbers given are 5 or 6 and these have binding energies close to those of the stepped surfaces. So it appears that once sites with co-ordination number of 7 or less are available other factors, such as cluster shape and charge state,

Table 3 Summary of calculated data for O_2 molecular adsorption to isolated Au_n clusters

Cluster	Method	$E_{ads}(O_2)$/ kJ mol^{-1}	Co-ord., Au C.N. [Au geom.]	Au···O–O, θ/degrees	O–O bond length/Å	Ref.
Au^-	PW91/L2DZ(Au)/6-311 + G(3df)(O)	42	η^1, 0	—	1.26	73
	B3LYP/L2DZ(Au)/6-311 + G(3df)(O)	21	η^1, 0	124	1.24	73
Au	PW91/L2DZ(Au)/6-311 + G(3df)(O)	44	η^1, 0	—	1.22	73
	B3LYP/L2DZ(Au)/6-311 + G(3df)(O)	1	η^1, 0	119	1.20	73
Au^+	PW91/L2DZ(Au)/6-311 + G(3df)(O)	77	η^1, 0	—	1.25	73
	B3LYP/L2DZ(Au)/6-311 + G(3df)(O)	47	η^1, 0	123	1.22	73
Au_2^-	PW91/L2DZ(Au)/6-311 + G(3df)(O)	120	η^1, 1	—	1.31	73
	PW91/STO TZP	140	η^1, 1	—	1.33	64
	B3LYP/SBKJC(Au)/6-31G(d,p)(O)	118	η^1, 1	—	—	74
	PBE/TM PPs/plane wave	134	η^1, 1	116	1.34	63
	B3LYP/L2DZ(Au)/6-311 + G(3df)(O)	92	η^1, 1	117	1.31	72
	CCSD(T)/SBKJC(Au)/6-31G(d,p)(O)	103	η^1, 1	115	1.30	74
Au_2	PW91/USPP/plane wave	47	η^1, 1	—	1.27	72
	PW91/L2DZ(Au)/6-311 + G(3df)(O)	34	η^1, 1	—	1.22	73
	B3LYP/L2DZ(Au)/6-311 + G(3df)(O)	6	η^1, 1	121	1.20	73
Au_2^+	PW91/L2DZ(Au)/6-311 + G(3df)(O)	45	η^1, 1	—	1.24	73
	B3LYP/L2DZ(Au)/6-311 + G(3df)(O)	27	η^1, 1	122	1.21	73
Au_3^-	PW91/STO TZP	48	η^1, 1 [lin.]	$90 < \theta < 180$	1.29	64
		121	η^1, 2 [2*D*]	—	—	
	PW91/L2DZ(Au)/6-311 + G(3df)(O)	32	η^1, 1 [lin.]	—	1.26	73
	B3LYP/L2DZ(Au)/6-311 + G(3df)(O)	4	η^1, 1 [lin.]	113	1.22	73
	CCSD(T)/SBKJC(Au)/6-31G(d,p)(O)	−37	η^1, 1 [lin.]	114	1.30	74
Au_3	PW91/USPP/plane wave	87	$\mu_{1,1}$, 2,2 [2D]	—	1.32	72
	BPW91/L2DZ(Au)/DZP(O)	80	η^1, 2 [2D]	$90 < \theta < 180$	—	76
		92	$\mu_{1,1}$, 2,2 [2D]	—		
	PW91/L2DZ(Au)/6-311 + G(3df)(O)	68	$\mu_{1,1}$, 2,2 [2D]	—	1.22	73
	B3LYP/L2DZ(Au)/6-311 + G(3df)(O)	24	$\mu_{1,1}$, 2,2 [2D]	—	1.21	73
	B3LYP/SBKJC(Au)/6-31G(d,p)(O)	18	η^1, 2 [2D]	—	—	74
	CCSD(T)/SBKJC(Au)/6-31G(d,p)(O)	8	η^1, 2 [2D]	107[c]	1.36	74
Au_3^+	PW91/L2DZ(Au)/6-311 + G(3df)(O)	41	η^1, 2 [2D]	—	1.29	73
	B3LYP/L2DZ(Au)/6-311 + G(3df)(O)	23	η^1, 2 [2D]	122	1.28	73
Au_4^-	PW91/STO TZP	112	η^1, 2 [2D]	$90 < \theta < 180$	1.32	64
	PW91/L2DZ(Au)/6-311 + G(3df)(O)	99	η^1, 2 [2D]	—	1.30	73
	B3LYP/L2DZ(Au)/6-311 + G(3df)(O)	69	η^1, 2 [2D]	115	1.30	73
Au_4	PW91/L2DZ(Au)/6-311 + G(3df)(O)	36	η^1, 2 [2D]	—	1.23	73
	B3LYP/ L2DZ(Au)/6-311 + G(3df)(O)	8	η^1, 2 [2D]	120	1.20	73
Au_4^+	PW91/L2DZ(Au)/6-311 + G(3df)(O)	32	η^1, 3 [2D]	—	1.25	73
	B3LYP/L2DZ(Au)/6-311 + G(3df)(O)	21	η^1, 3 [2D]	$90 < \theta < 180$	1.20	77
	B3LYP/L2DZ(Au)/6-311 + G(3df)(O)	16	η^1, 3 [2D]	122	1.21	73
Au_5^-	PW91/ STO TZP	38	η^1, 2 [2D]	$90 < \theta < 180$	1.36	64
	PW91/L2DZ(Au)/6-311 + G(3df)(O)	42	η^1, 2 [2D]	—	1.27	73
	B3LYP/L2DZ(Au)/6-311 + G(3df)(O)	5	$\mu_{1,1}$, 3,3 [2D]	—	1.41	77
	B3LYP/L2DZ(Au)/6-311 + G(3df)(O)	7	η^1, 2 [2D]	124	1.25	73
Au_5	PW91/L2DZ(Au)/6-311 + G(3df)(O)	98	$\mu_{1,1}$, 3,3 [2D]	—	1.23	73
	PBE/TM/DZP(Au)/DZP(O)	88	$\mu_{1,1}$, 3,3 [2D]	—	1.35	80
	B3LYP/L2DZ(Au)/6-311 + G(3df)(O)	62	$\mu_{1,1}$, 3,3 [2D]	—	1.21	73
	B3LYP/L2DZ(Au)/6-311 + G(3df)(O)	70	$\mu_{1,1}$, 3,3 [2D]	—	1.31	77
Au_5^+	PW91/L2DZ(Au)/6-311 + G(3df)(O)	35	η^1, 2 [2D]	—	1.33	73
	B3LYP/L2DZ(Au)/6-311 + G(3df)(O)	16	η^1, 2 [2D]	121	1.31	73
Au_6^-	PW91/STO TZP	90	η^1, 2 [2D]	$90 < \theta < 180$	1.32	64
	PW91/L2DZ(Au)/6-311 + G(3df)(O)	97	η^1, 2 [2D]	—	1.30	73
	B3LYP/L2DZ(Au)/6-311 + G(3df)(O)	75	η^1, 2 [2D]	116	1.31	73
Au_6	PW91/L2DZ(Au)/6-311 + G(3df)(O)	14	η^1, 2 [2D]	—	1.22	73
	PBE/TM/DZP(Au)/DZP(O)	14	η^1, 2 [2D]	115	1.26	80
	B3LYP/L2DZ(Au)/6-311 + G(3df)(O)	0	η^1, 2 [2D]	123	1.20	73
Au_6^+	PW91/L2DZ(Au)/6-311 + G(3df)(O)	39	η^1, 2 [2D]	—	1.24	73
	B3LYP/L2DZ(Au)/6-311 + G(3df)(O)	9	η^1, 2 [2D]	124	1.20	73
Au_7	PBE/TM/DZP(Au)/DZP(O)	50	η^1, 2 [2D]	116	1.28	80
Au_8	PBE/TM/DZP(Au)/DZP(O)	19	η^1, 2 [2D]	122	1.26	80
Au_9^-	B3LYP/L2DZ(Au)/DZP(O)	17	η^1, 4 [3D]	$90 < \theta < 180$	—	78
Au_9	PBE/TM/DZP(Au)/DZP(O)	52	η^1, 3 [2D]	119	1.28	80
Au_{10}^-	B3LYP/L2DZ (Au)/DZP(O)	80	$\mu_{1,1}$, 3,3 [3D]	—	1.37	78
	B3LYP/L2DZ(Au)/D95V + pd(O)	8	η^1, 5 [3D]	122	1.25	94

Table 3 (*continued*)

Cluster	Method	$E_{ads}(O_2)$/ kJ mol^{-1}	Co-ord., Au C.N. [Au geom.]	Au···O–O, θ/degrees	O–O bond length/Å	Ref.
Au_{10}	B3LYP/L2DZ(Au)/D95V + pd(O)	1	η^1, 5 [3D]	126	1.22	94
	PBE/TM/DZP(Au)/DZP(O)	27	η^1, 3 [2D]	119	1.27	80
Au_{10}^+	B3LYP/L2DZ(Au)/D95V + pd(O)	No inter.	—	—	—	94
Au_{11}^-	B3LYP/L2DZ(Au)/DZP(O)	21	$\mu_{1,1}$, 3,3 [3D]	—	—	78
Au_{13}	B3LYP/L2DZ(Au)/L2DZ + pd(C,O)	10	η^1, 5 [3D]	119	1.25	61

[a] Method includes functional/Au basis and ECP/O basis and ECP, with L2DZ = LANL2DZ, DZP, TZP = double, triple zeta plus polarisation basis set, STO = Slater type orbitals used without ECPs but with the core states frozen, most other simulations use the standard Gaussian basis as indicated. For pseudopotentials: TM = Troullier-Martins, USPP = ultra soft pseudopotentials, PAW = projector augmented waves, CCSD(T) geometries are taken from MP2 optimisations. [b] In addition to the co-ordination modes described in the text, $\mu_{1,1}$ = side-on O_2, bridging 2 Au atoms, Au co-ordination refers to the number of neighbours in the cluster for the co-ordinated Au, for bridging modes two values are given. [c] For this one case the O_2 molecular axis is out of the plane defined by the Au cluster.

become more important than the number of neighbours an Au atom has.

Oxygen adsorption

Molecular oxygen has a triplet ground state with the unpaired electrons occupying the degenerate anti-bonding $2\pi_u^*$ orbitals formed by the O(2*p*) atomic orbitals perpendicular to the molecular axis. Transfer of charge to the electrophilic O_2 molecule can lead to a series of species covering the superoxo anion, O_2^- (doublet), and the peroxy anion O_2^{2-} (singlet). As charge is added the population of the anti-bonding orbitals must increase and so the bond length increases accordingly. This means that, in a calculation, the bond length, charge state and overall excess spin density of a surface bound O_2 species can all help its classification.[69] As mentioned in section 2 the multiplicity of the electronic state is not well defined in DFT, however in unrestricted spin calculations the difference between the spin up and spin down densities is usually quoted.

Molecular adsorption of oxygen on metal surfaces has been observed using low temperature NEXAFS spectra.[70] A superoxo species was identified on Pt(111) with an O–O bond length of 1.32 ± 0.05 Å, while on Ag(110) a peroxy anion adsorbate with O–O = 1.47 ± 0.05 Å was observed at 100 K. These measurements show the expected increasing bond length of O_2 from the gas phase value[71] of 1.207 Å as the anti-bonding orbitals of the molecule are occupied.

Table 3 gives some examples of calculations on the Au_n/O_2 system using various functionals, basis sets and core representations. Data is drawn from studies that have directly considered the effect of cluster size and charge state on O_2 adsorption. Neutral Au_1 adsorbs O_2 molecules more weakly than either the anionic, Au_1^-, or cationic, Au_1^+. The B3LYP results show that the adsorption energy is less than 10 kJ mol^{-1} for the neutral Au, about 20 kJ mol^{-1} for the anionic Au and 47 kJ mol^{-1} for the cationic Au. In all three cases, the O–O bond lengths remain close to the equilibrium value for the isolated O_2 molecule which, using PW91 and a plane wave basis is 1.238 Å,[72] and at the B3LYP level is 1.20 Å,[73] in good agreement with the experimental value. The PW91 results give adsorption energies which are larger by about 20 kJ mol^{-1}, and the O_2 bond tends to be longer by around 0.02 Å than for the hybrid functional. This is consistent with the tendency of the PW91 functional to overbind since the bonding mechanism discussed below involves charge transfer from Au to O_2 anti-bonding orbitals.

For Au_2, the neutral cluster again has the weakest O_2 adsorption (B3LYP: 6 kJ mol^{-1}), but the adsorption energy for the anionic cluster at the same level of theory (92 kJ mol^{-1}) is now greater than for the cationic cluster (27 kJ mol^{-1}). The strong O_2 adsorption on the anionic cluster is accompanied with a bond length increase to 1.31 Å. For anionic Au_2^- the pure gradient corrected functionals (PBE and PW91) give larger adsorption energies than the hybrid functional B3LYP. In addition the higher level CCSD(T) technique has been applied to this system,[74] so that the effect of including dynamic as well as static correlation can be seen to give an E_{ads} value intermediate between the B3LYP results and in good agreement with the experimental estimate of 97 ± 14 kJ mol^{-1}.[75] The CCSD(T) results were obtained for structures optimised at the MP2 level, a post-Hartree–Fock correlation method. The geometry obtained at this level does show good agreement with the GGA-DFT results, indicating that the geometries of the DFT calculations are reliable even if the adsorption energy is overestimated by up to 36%.

We have seen that the Au_3 cluster can be linear or triangular (with Jahn–Teller distortions), in Table 3 triangular structures are marked as [2D]. For anionic Au_3^- most DFT studies have concentrated on the ground state linear cluster. Terminal co-ordination of O_2 gives a weak adsorption of around 30–40 kJ mol^{-1} using PW91 and only 4 kJ mol^{-1} with the hybrid functional B3LYP with only small changes in the O_2 bond length compared to the respective reference calculations. For the 2D structure Yuan and Zeng have reported a much stronger interaction with E_{ads} = 121 kJ mol^{-1} based on the PW91 functional.[64] However, they comment that the linear structure of this anion has an energy 1.22 eV lower than the triangular form and so the latter would not be observed in gas phase clusters. The CCSD(T) result for $[Au_3O_2]^-$ actually shows a negative binding energy, so that although the structure is a local minimum its total energy is higher than the Au_3^- cluster and O_2 molecule in isolation. The geometries used by Gordon and co-workers comes from relaxation at the MP2 level since the computational expense of optimisation at the CCSD(T) level is prohibitive. This gives a 2D structure with a large apex angle

(131°) and the O_2 molecule bound to a basal Au atom. This is intermediate between the linear and the 2D structures used by Yuan and Zeng. The difference in geometry cannot explain the difference in sign of the adsorption energy between the methods, but given the near zero value from B3LYP it appears that the overestimation of binding energies using gradient corrected DFT is enough to swing the sign positive in this case.

Neutral Au_3 clusters can adsorb O_2 in either the η^1, end-on geometry seen for Au_3^- and all smaller clusters, or in a $\mu_{1,1}$, side-on mode. The BPW91[76] and B3LYP results show that $\mu_{1,1}$ co-ordination has a higher adsorption energy, if values obtained using the same functional are compared. The CCSD(T) structure reported in this case is unusual in that the axis of the O_2 molecule is out of the plane while for all other structures the O_2 molecule is co-planar with the Au atoms.

The smallest anionic cluster for which the $\mu_{1,1}$ is reported[77] is Au_5^- although, as explained below, the even number of electrons on this cluster leads to a low adsorption energy for O_2.

As the cluster size increases, the differences between the adsorption energies for the neutral, anionic and cationic clusters become smaller. This is because the charge is spread out over a larger number of atoms. The cluster geometry also changes as the size increases. For clusters from Au_9 3D geometries are used despite the energetic preference for planar Au particles up to Au_{14} according to DFT (Fig. 4). On these larger clusters O_2 adsorption energies are only high for cases with an odd number of electrons and preferably a negative charge.[78] The 3D geometries are usually adopted to reflect the shapes seen for larger particles in electron microscopy of catalysts.

Fig. 10 shows the calculated adsorption energies for neutral and anionic Au clusters for molecular and dissociative adsorption of O_2 as a function of the number of Au atoms in the cluster from the work of Häkkinen and co-workers.[79] In this study the PBE functional with norm-conserving pseudopotentials and adapted molecular dynamics was used to identify energy minima. For Au_2, dissociative adsorption to the neutral cluster is actually endoergodic, with the cluster $+O_2$ total energy almost 40 kJ mol^{-1} higher than the isolated components. The Au–O bonds formed by the atomic oxygen product are insufficient to compensate for the loss of the gas phase O_2 bond energy. All other clusters show favourable adsorption energies for all charge states for both molecular and dissociative adsorption modes. Generally, the adsorption to the negatively charged clusters is stronger than to the neutral counterparts. For Au_2^- and Au_3^- molecular adsorption leads to more favourable energies than does dissociation, however the order swaps for larger cluster sizes and the same effect is observed for the neutral clusters. For Au_4 and above there is a clear oscillation of adsorption energy with the number of atoms in the cluster with even numbered clusters giving energies around 50 kJ mol^{-1} higher than odd clusters for anionic Au_n^-, while neutral clusters give dissociative adsorption energies which favour odd numbers of Au atoms over even. Table 3 shows that this preference for adsorption to clusters with an unpaired electron continues to anion cluster sizes of 10 Au atoms. However, the effect is not present for molecularly adsorbed O_2 in the neutral cluster case. The $5d^{10}6s^1$ valence shell of Au will lead to even anionic structures and odd neutral structures having a single unpaired electron and it is this which Häkkinen suggests gives the observed oscillations.

Fig. 11 shows the spin density difference for the Au_6 clusters taken from the same paper. The spin unrestricted calculation gives density contributions from spin-up and spin-down electrons separately. The map of the difference between these shows where the un-paired electrons reside. In isolated molecular O_2 the triplet state would give excess spin-up electron density in the $2\pi_u{}^*$ orbitals formed from the off-axis $O(2p_x)$ and $O(2p_y)$ atomic orbitals, at right angles to one another. Fig. 11a shows that this is largely preserved in the Au_6O_2 case, there is a ring structure around the axis of the O_2 molecule from the single occupancy of these two molecular orbitals. For the neutral cluster the adsorption energy is correspondingly weak and the O_2 bond length is hardly altered from the reference gas phase calculation at the same level of theory (1.268 *cf.* 1.250 Å). The anionic Au_6^- gives

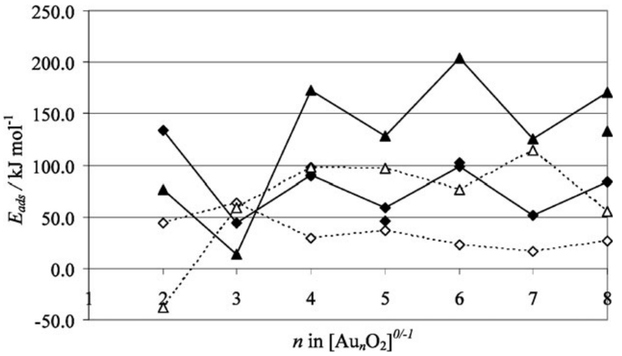

Fig. 10 Calculated adsorption energy for O_2 as a function of Au cluster size. Data for neutral Au_n clusters is shown with open symbols, triangles for dissociative adsorption, diamonds for molecular adsorption and dotted lines. Data for anionic Au_n^- clusters is shown using solid symbols and solid lines, again using triangles for dissociative adsorption, diamonds for molecular adsorption. For values of n for which results for alternative geometries are available these are plotted to show the range of data. Values taken from ref. 79.

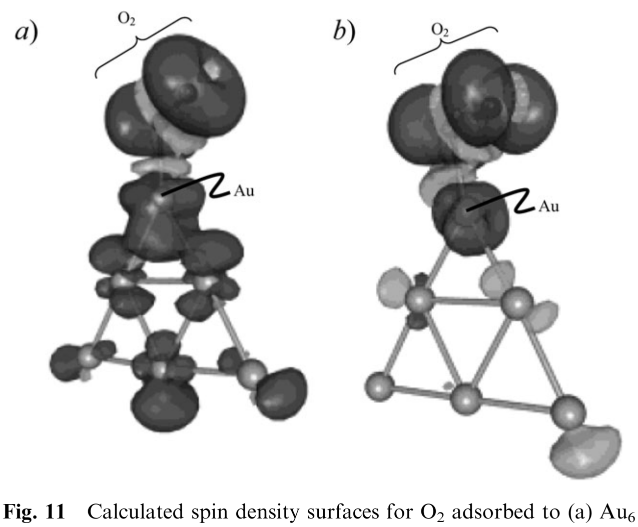

Fig. 11 Calculated spin density surfaces for O_2 adsorbed to (a) Au_6 and (b) Au_6^-. Reprinted in part with permission from ref. 79. Copyright 2003 American Chemical Society.

the highest molecular adsorption energy of any of the clusters studied. The spin density shown in Fig. 11b shows a localised interaction between the co-ordinating Au atom and one of the oxygen atoms. The ring feature on the O_2 adsorbate is no longer present because the $2\pi_u$* orbital in the Au–O_2 plane does not show up in the spin density. This suggests that either the single electron from this orbital has been re-distributed to the cluster, or that the single unpaired electron of the Au_6^- cluster has been donated to the O_2 species and so the in-plane $2\pi_u$* contains spin-paired electrons. The calculated charge on O_2 in this structure is -0.745 $|e|$ and the bond length is 1.362 Å, so that the donation is from the negative cluster to the anti-bonding O_2 molecular orbital to give a superoxo species. Correspondingly, calculated vibrational frequencies for O_2 adsorbed to even numbered anionic Au clusters show a decrease relative to O_2 in the gas phase.[80] This bonding model is consistent with the observation from Table 3 that the Au–O–O angle for all clusters with η^1 co-ordination is less than 180°. This allows σ-symmetry Au–O_2 orbital overlap with the oxygen molecule $2\pi_u$* orbital. The bridging $\mu_{1,1}$ geometries listed in Table 3 also allow efficient donation into the empty molecular orbitals of the O_2 molecule. For example Mills *et al.*[72] have used periodic DFT (PW91) to investigate the interaction of O_2 with small Au clusters. The charge density difference plot for the Au_3O_2 structure with $\mu_{1,1}$ co-ordination ($\rho(Au_3O_2)-\rho(Au_3)-\rho(O_2)$) is shown in Fig. 12, and this also demonstrates a density gain in the O_2 $2\pi_u$* orbital in the Au_3 plane. The adsorption energy for O_2 in this structure is 87 kJ mol^{-1}.

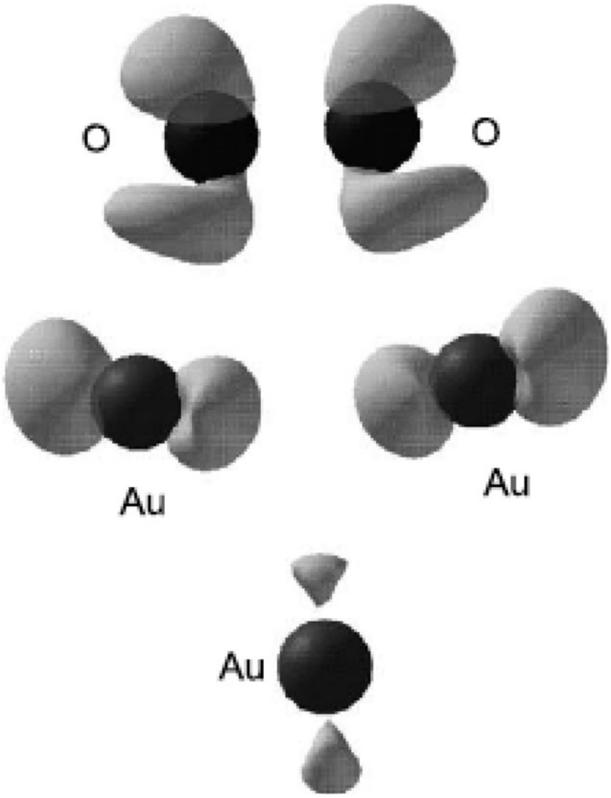

Fig. 12 Calculated density difference for Au_3O_2 with O_2 in a $\mu_{1,1}$ co-ordination. Reused with permission from ref. 72. Copyright 2002, American Institute of Physics.

The calculated barriers for conversion of the molecularly adsorbed O_2 to the dissociated state starting from the structures of Fig. 11 are 225 kJ mol^{-1} (Au_6^-) and 322 kJ mol^{-1} (Au_6). So that, while activation by charge transfer from the anionic cluster does lead to a lower barrier than for the neutral particle, the energy required to desorb the molecule is considerably less than that required to break the O_2 bond in both cases.

The adsorption of di-oxygen to Au_n^- clusters has been studied experimentally by Whetten and co-workers,[81] using pulsed helium flow-reactor methods. They conclude that even numbered clusters from $n = 2$ to 20 adsorb at most one molecule of O_2, while odd numbered clusters do not exhibit measurable adsorption. They show that this behaviour is correlated with the electron affinity of the Au clusters, as would be expected from the odd/even electron counts for even/odd anionic clusters. For the gradient corrected DFT methods multiple adsorption of O_2 has been reported based on PW91 results. However, this is likely due to the overbinding noted above when comparing this functional to hybrid or explicitly correlated methods.

Not too surprisingly, periodic DFT calculations for the adsorption of O_2 to the surfaces of bulk Au find a generally very weak physisorbed state. For the flat Au(111) surface, in which atoms have a co-ordination number (CN) of 9, the GGA-DFT calculated value is practically zero.[82] The interaction of O_2 with the surface does increase when low co-ordination sites are made available through the use of high index Miller planes.

Hu and co-workers[68] have studied the adsorption of O_2 to the stepped surfaces Au(221), Au(211) using the PBE functional and large core ultrasoft pseudopotentials, leaving 11 Au valence electrons ($6s^1 5d^{10}$). The (221) surface consists of (111) terraces with (111) step edges on which Au atoms have a CN of 7. The (211) surface also has Au atoms with CN = 7 and (111) terraces, but the step edges are orientated to include the more open (100) facet. By removing atoms from the step edges lower co-ordination atoms were exposed at kink sites with CN = 6. The effect of CN on the d-orbital energy of surface Au

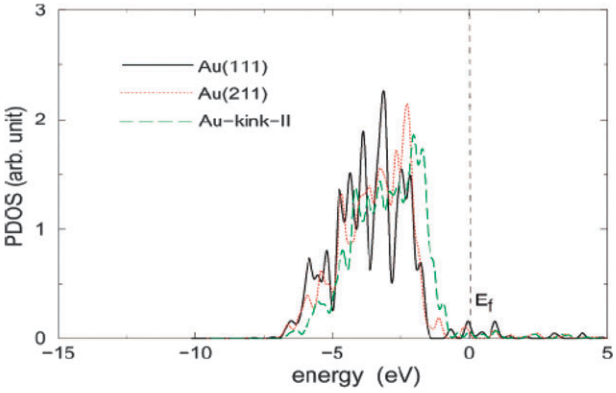

Fig. 13 The partial density of states for Au d-orbitals of atoms on the Au(111) which have CN = 9, Au(211) with CN = 7 and a kink site with CN = 6. Reprinted with permission from ref. 68. Copyright 2002 American Chemical Society.

atoms can be seen by plotting the partial density of states (PDOS) for the d-states of particular atoms. Fig. 13 shows the resulting PDOS which indicates that the d-band edge moves to higher energy for the low co-ordinate atoms. This may be expected to lead to stronger binding of atomic adsorbates as the localised d-orbitals at the low co-ordination sites are nearer to the Fermi level and so more available to mix with the orbitals of surface species.[83] However, for atomic oxygen, Hu observes a maximal adsorption energy on the 7 co-ordinate atoms of the Au(211) surface with E_{ads} = 298 kJ mol^{-1}, referenced to the free O atom. While this is sufficient to overcome the O_2 bond energy (531 kJ mol^{-1} at the PBE level), it is considerably less than found by the same methodology for Pt(111), E_{ads} = 415 kJ mol^{-1}.[84] The bonding model put forward for O atoms consists of an ionic interaction from charge donated from the surface to the adsorbed atom and a covalent component involving orbital mixing. The ionic contribution will involve the s/p states at the metal Fermi level, while the covalent component depends on the more localised Au d-states. The covalent part of the interaction will increase with decreasing co-ordination number, since Fig. 13 shows that these states move upward in energy and so mix more efficiently with the O atom orbitals. However the d-states are still below the Fermi level and so are filled, making the covalent contribution to the bond energy small. Hu estimates this to be around 10 kJ mol^{-1} from a simple extended Hückel argument. The ionic interaction is then assessed using Mulliken analysis to give Au atom charges, demonstrating a decrease in electron population with CN. Accordingly, as CN is reduced the covalent interaction between Au and O gets stronger, but the electron density available to donate to the adsorbate atom also reduces, making the ionic interaction weaker. These competing effects could lead to the observed maximal adsorption energy for O atoms.

This model is also likely to have an impact on the location of molecular oxygen adsorption to Au particles. We have seen that this also depends on electron donation from the surface to the adsorbate and so low co-ordination Au atoms may not be optimal for oxygen adsorption. Hu does not report the adsorption energy of O_2 but does consider the barrier to bond cleavage to form atomically adsorbed species. The O_2 dissociation barrier is high on all the Au systems studied with the lowest value found for the Au(211) step edge site with a barrier of 90 kJ mol^{-1}. In the transition state one oxygen atom is moving toward the favourable step bridge site discussed above, while the other atom ends up in an fcc hollow site of the (111) terrace at the foot of the step. Although the adsorption energies for the atomic species suggest that the bond cleavage is thermodynamically favourable, this barrier is too high to allow for atomic oxygen produced by direct activation of O_2 on Au surfaces at the low temperatures used for CO oxidation.

For surfaces stretched by 10%, to mimic the strain imposed by an interface to an oxide support the adsorption energies do become more favourable.[82] To show this the strained and unstrained Au(111) and Au(211) surfaces have been compared at the GGA-PW91 level using a plane-wave basis set with the USPP representation of the core states. On Au(111) even the strained surface gives an estimated adsorption energy of only 8 kJ mol^{-1}. The Au(211) relaxed termination is slightly better at 14 kJ mol^{-1}, becoming 25 kJ mol^{-1} with an imposed 10% lattice expansion. However, in the same calculations the barriers to O_2 dissociation are all considerable with the lowest barrier calculated for the strained Au(211) surface at 61 kJ mol^{-1}. This means that molecular O_2 will be weakly adsorbed and the effective barrier to desorption is significantly lower than that for dissociation. In the absence of the support, the larger Au catalyst particles represented by these periodic calculations will have only a low population of molecular oxygen adsorbed.

In contrast to Au, PW91 calculations using a plane wave basis set to consider O_2 adsorption to Ag(110) give an adsorption energy of 53 kJ mol^{-1} with an adsorbate bond length of 1.45 Å.[85] Charge analysis shows this to be a peroxy like state with a calculated spin polarisation of 0.12. The barrier for dissociation from this species is 60 kJ mol^{-1} with a O···O distance in the transition state of 2.22 Å. In the same study no barrier was found for direct adsorption into the dissociated chemisorbed state. This contradicts experimental molecular beam experiments which shows no direct dissociative chemisorption on Ag(110) below incident kinetic energies of 1 eV.[86] In the discussion of this point doubts were raised regarding the accuracy of density functional theory to describe the weak interactions when O_2 is far from the surface. The dissociation *via* the peroxy route involves bond cleavage from a starting point in which molecular oxygen is already interacting with the surface in a chemisorption mode and so is likely to be better described by DFT.

For oxygen adsorption to Au both the cluster and periodic models show that molecular adsorption is weak unless there is significant charge donation into one of the O_2 $2\pi_u$* orbitals. For clusters negatively charged Au_n^- with n even lead to the strongest molecular adsorption energies since the unpaired electron is in a high energy level and can be effectively donated to form an O_2^- superoxo species. For periodic surfaces the Au(111) surface is unreceptive to oxygen but stepped surfaces, particularly if strained, can give favorable molecular adsorption. Dissociation on all but the smallest particles is thermodynamically favorable, but the calculated barriers are considerably higher than the energy required for desorption of the molecular species.

CO oxidation mechanism on isolated Au particles

There are two basic mechanisms that have been considered in most of the current literature on the simulation of CO oxidation over Au particles. These differ in the adsorption process for O_2. Dissociative adsorption gives the elementary steps:

$$O_2(g) \rightarrow O_2(a) \qquad \text{(i)}$$

$$O_2(a) \rightarrow 2O(a) \qquad \text{(ii)}$$

$$CO(g) \rightarrow CO(a) \qquad \text{(iii)} \qquad \text{(Scheme 1)}$$

$$CO(a) + O(a) \rightarrow CO_2(a) \qquad \text{(iv)}$$

$$CO_2(a) \rightarrow CO_2(g) \qquad \text{(v)}$$

Where the letters in brackets indicate gas phase, (g) or adsorbed states, (a). Alternatively the O_2 bond can be broken during the formation of the new C–O bond *via* an intermediate state with molecular oxygen bound to CO:

$$\begin{array}{lll}
O_2(g) \rightarrow O_2(a) & \text{(i)} & \\
CO(g) \rightarrow CO(a) & \text{(ii)} & \\
O_2(a) + CO(a) \rightarrow O_2 \cdots CO(a) & \text{(iii)} & \text{(Scheme 2)} \\
O_2 \cdots CO(a) \rightarrow CO_2(a) + O(a) & \text{(iv)} & \\
CO_2(a) \rightarrow CO_2(g) & \text{(v)} &
\end{array}$$

Lopez and Nørskov,[87] based on RPBE calculations with ultrasoft pseudopotentials and the Au(7,3) cluster, suggest that Scheme 1 is competitive with Scheme 2. Although it is difficult to differentiate the two pathways on the small cluster used in their calculations. In Scheme 1 the O_2 bond cleavage takes place from a starting point with the oxygen molecule adsorbed in a $\mu_{1,1}$ fashion on the base of the clusters (100) face (foreground of Fig. 5). The CO molecule is simultaneously adsorbed to one of the Au atoms in the 3-layer on the same square face. After the separation to two O atoms the CO molecule has moved downward toward one of the atomically adsorbed oxygen atoms. The movement of CO as the O_2 bond breaks suggests that it is involved in stabilising the transition state for bond cleavage to give a lower barrier than found for O_2 on Au alone. The atomic oxygen then adds to CO to form carbon dioxide. In Scheme 2 the O_2 cleavage occurs simultaneously with O···CO bond formation (step (iii)), so that there is only a single transition state between the co-adsorbed molecules and the product. Either way, the highest barrier on the potential energy surface for the reaction is below 40 kJ mol^{-1}, and so consistent with experimental kinetics.

The weak adsorption of O_2 found for neutral and positively charged clusters would suggest that Scheme 2 is likely the initial oxidation route, although the O(a) species formed at step (iv) can go on to oxidise further CO(a) following step (iv) of Scheme 1. Temporal analysis of products (TAP) experiments using O isotope labeling also show no exchange of oxygen with the oxide lattice for Au/TiO_2, suggesting that it is molecular, rather than atomic, oxygen that is involved in the reaction.[88]

Scheme 2 has also been considered for Au surfaces using periodic calculations. Hu and co-workers (PBE functional) used the step edge on the Au(211) surface as a model low coordination site.[68] The reaction of O_2 with CO at the step edge is initiated by the formation of an $O_2 \cdots CO$ orientated complex, with molecules on adjacent step edge atoms. The formation of this intermediate is rate limiting and the calculated barrier is reasonably low, 44–57 kJ mol^{-1}, depending on CO coverage, with the lower barrier for higher coverage. CO was also shown to react with atomic O at an Au step site with an even low energy barrier of 24 kJ mol^{-1}.

Co-operative adsorption of O_2 and CO has also been studied for isolated anionic cluster models. For Au_2^- Socaciu *et al.*[89] have used mass spectrometry of gas phase ions along with PBE calculations to suggest a pathway involving the formation of a carbonate anion:

$$\begin{array}{lll}
Au_2^- + O_2 \rightarrow Au_2O_2^- & \text{(i)} & \\
Au_2O_2^- + CO \rightarrow Au_2CO_3^- & \text{(ii)} & \\
Au_2CO_3^- + CO \rightarrow Au_2^- + 2CO_2 & \text{(iii)} & \\
Au_2O_2^- + CO \rightarrow Au_2COO_2^- & \text{(iv)} & \text{(Scheme 3)} \\
Au_2COO_2^- + CO \rightarrow Au_2CO_2^- + CO_2 & \text{(v)} & \\
Au_2CO_2^- \rightarrow Au_2^- + CO_2 & \text{(vi)} &
\end{array}$$

In the first step the O_2 molecule binds in an end-on configuration with the four atoms of the $Au_2O_2^-$ intermediate coplanar. Partial charge transfer from the Au_2^- species suggests a superoxo O_2^- "adsorbed" state. In step (ii) gas phase CO inserts into the O–O bond to form a carbonate anion bound by one oxygen to the Au_2 dimer. This insertion has a calculated barrier of only 29 kJ mol^{-1}. Capture of another CO molecule at a free carbonate oxygen then leads to the formation of $2CO_2$ molecules in step (iii). Alternatively, CO can insert into the Au–O bond of the $Au_2O_2^-$ complex to give a peroxyformate like species in step (iv). Addition of a further CO molecule to the terminal oxygen of the peroxy group then leads to stepwise formation of $2CO_2$ molecules in steps (v) and (vi) with similar calculated barriers to the CO insertion into O–O route.

These calculations illustrate that CO oxidation on neutral or anionic Au can provide pathways that are at least consistent with the low energy activation barriers measured by Haruta (34 kJ mol^{-1} for Au/TiO_2).[90] However the low adsorption energy of molecular oxygen for neutral and cationic clusters or periodic surfaces would lead to the conclusion that, at normal temperatures, the supply of oxidant should be limiting.

Water

Moisture has been shown to increase the catalytic activity for Au catalysed oxidation of CO by two orders of magnitude or more.[91,92] The dissociation barrier for H_2O on Au(111) has been calculated using the PBE functional and a plane wave basis set, giving 216 kJ mol^{-1}, which is 28 kJ mol^{-1} higher than found for Ag(111).[93] In the presence of pre-adsorbed O the barrier on Au(111) drops to 59 kJ mol^{-1}. The preferred site for the atomic oxygen is a three fold hollow site and water adsorbs on a neighboring top site forming an O–H···O(a) hydrogen bond. Dissociation then leads to two surface hydroxyl groups. Schemes (1) and (2) both generate O(a) on the surface of Au particles and so with water present these could lead to hydroxyl groups even on the un-reactive Au(111) surface.

The formation of superoxide species on adsorption of O_2 to negatively charged clusters suggests that an alternative role for H_2O is to stabilise surface molecular oxygen form through hydrogen bonding.[61] Okumura *et al.*[94] have pursued this idea by performing unrestricted hybrid DFT (UB3LYP) calculations on Au_{10}(7,3) clusters with adsorbed O_2 and H_2O. The LANL2DZ ECP and basis set was used for the Au atoms. To obtain a cluster with energy minimised Au–Au interactions they first relaxed a cubooctahedral Au_{13}(3,7,3) cluster, from which the $Au_{10}(7,3)$ structure was cut and then fixed for subsequent calculations. This means that any effects due to fluxional changes of the cluster in response to the adsorbates will be neglected and adsorption energies are thus lower limits. For a neutral cluster Mulliken charges indicated that the surface Au atoms actually carry small negative charges, while the central Au in the 7-atom layer is positive. Anionic and cationic Au_{10} clusters were also investigated by simply adjusting the total charge of the system. As discussed earlier, an important problem is to account for the reaction when the adsorption of O_2 is so weak. The Au_{10}^+ cluster had a negligible interaction with O_2 while the adsorption energies for Au_{10} and Au_{10}^- clusters were 1.4 and 8.2 kJ mol^{-1}, respectively. The calculated charge densities show that there is charge transfer from the Au_{10} and Au_{10}^- clusters to the O_2 leading to the favourable, if low, adsorption energies. All three clusters were shown to have an interaction with H_2O, with the largest adsorption energy for the Au_{10}^+ cluster. Mulliken charge analysis indicates charge donation from the H_2O molecule to the Au clusters through geometries orientating the oxygen lone pair toward the low co-ordination Au atoms in the 3-atom layer. This means that the presence of H_2O molecules increases the negative charge at the surface of the Au cluster, which then promotes the adsorption of O_2. In addition hydrogen bonding, $O_2^{\delta-}\cdots H_2O$, further stabilises the adsorption of di-oxygen in the presence of water.

This model of water adsorption to an Au cluster has also been considered by Bongiorni and Landman.[95] They find that H_2O can adsorb to Au_8 ($E_{ads} \leq 29$ kJ mol^{-1}) or Au_{30} ($29 \leq E_{ads} \leq 58$ kJ mol^{-1}). In presence of H_2O, O_2 adsorbs to sites it to which it would not do so alone, *e.g.* top sites away from the "oxide interface". The co-adsorption of O_2 and H_2O gives a binding energy to Au_8 in the range 39–87 kJ mol^{-1}, whereas there are no bound adsorption geometries found for O_2 alone. In the dimer calculation O_2 adsorbs in a singlet state (peroxy) O_2^{2-} and forms an H-bond with the co-adsorbed water molecule. They also find similar co-adsorbed structures for Au_8 supported on MgO(100). For this system the reaction with CO was followed. Proton transfer from water to the adsorbed peroxy anion gives a hydroperoxyl like surface species. Direct adsorption of CO to the OH end of this intermediate gives an Eley–Rideal transition state with a barrier to CO_2 formation of only 48 kJ mol^{-1}. Desorption of CO_2 is accompanied by return of the proton to form water and O(a) on the Au cluster surface. This implies that water is not consumed in the reaction and so could be effective in small quantities. This water assisted reaction takes place on the Au cluster surface without the direct involvement of the MgO support.

5. The interaction of Au with oxide supports

Background

The preparation of Au catalysts for experimental programs differs between the catalytic and surface science communities. The catalysts that are used in reactor work are typically high surface area oxides onto which Au is deposited from an aqueous salt and then calcined in air at elevated temperatures prior to use.[96] The species in solution are negatively charged complexes of Au^{3+} derived from auric acid $HAuCl_4$ and the deposition process to generate Au/TiO_2 catalysts has been shown to be pH dependent.[97] Up to the isoelectric point of TiO_2 (pH 6) the surface is positively charged due to the presence of hydroxyl groups, allowing electrostatic forces to bind the anionic Au solution species to the surface. However, the cluster sizes produced are large, and the catalysts not as active, as those generated at higher pH. Above the isoelectric point the surface will be negatively charged and deposition is *via* neutral $Au(OH)_3{\cdot}H_2O$.[98] This gives higher particle dispersion, reduces the inclusion of detrimental Cl, and generates particles in the 1.5–4 nm range. There is an ongoing debate as to the active form of Au in these catalysts, but it is clear from experiments monitoring oxidation state with XANES spectroscopy that both zero valent and oxidised Au species are present in working catalysts, at least for the Au/MgO system.[99]

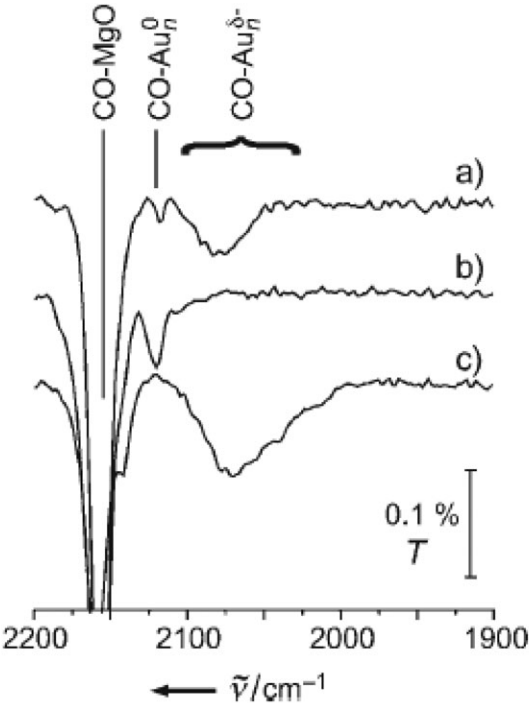

Fig. 14 Infra-red spectra for Au supported on MgO films after saturation coverage with CO differing in the pre-treatment of the film prior to Au deposition. (a) MgO film pre-treated with medium-dose electron bombardment, (b) pristine MgO film and (c) MgO film pre-treated with high-dose electron bombardment. From ref. 100. Copyright (2006) Wiley-VCH Verlag GmbH & Co. KGaA. Reproduced with permission.

In surface science experiments Au clusters are deposited onto well-defined oxide surfaces using vapour deposition under ultra-high vacuum conditions. In this case the Au clusters are ready formed in the gas phase and find binding sites on the oxide surface without the intervention of aqueous chemistry. Oxide films are grown on metal substrates as model supports. The films can be prepared in near pristine form through careful annealing. To investigate the influence of defects these films can then be deliberately degraded by electron bombardment.

Studies of Au deposited on MgO(100) prepared in this way show differences in the IR bands from CO adsorbed to Au particles on the pristine and those from Au on the defective films. Fig. 14 shows an example series of spectra reported by Freund and co-workers.[100] For all films, an intense signal consisting of a doublet of lines at 2163 and 2153 cm^{-1} is seen. This is characteristic of CO adsorbed on the MgO surface. For the pristine film with deposited Au an additional band at 2120 cm^{-1} appears, as expected for CO on small neutral Au clusters (Table 2). This is slightly blue-shifted compared to CO on large clusters or on single crystal surfaces of Au. For the defective films a broad feature is seen which spreads from 2100 to 2000 cm^{-1} for the most heavily bombarded case. This feature is red shifted with respect to CO on Au crystal surfaces or neutral Au particles and indicates adsorption to $\mathrm{Au}_n^{\delta-}$ clusters. These experimental results suggest that on bombarded films the Au clusters pick up charge from the defect centres. Red shift occurs because of greater π-back donation from the negatively charged clusters and a broad spread is seen because different size clusters spread out the δ^- charge differently, *i.e.* the effect reduces with increasing cluster size. The theoretical work on CO adsorbed to neutral and anionic Au clusters in Table 2 shows a similar relationship between the relative positions of the IR bands, however the particle size range is too small to comment on the spread of values for anionic clusters. In experimental work by Yoon *et al.*[101] it is also shown that $\mathrm{Au}_n^{\delta-}$ trapped at defect centres on MgO(100) are catalytically active for CO oxidation, while Au_n on pristine films are inert.

Simulation of Au on oxides

The most popular materials for use in simulation studies of the interaction of metal particles with the oxide component of the catalyst are MgO, as a non-reducible support, and TiO_2 as a reducible support. In both cases the surface and defect structure of the oxides alone have been studied with a broad range of simulation techniques.[102–104] Magnesium oxide has the rock salt structure and the most stable surfaces are the MgO{100} family which correspond to the faces of the well known cubic unit cell. Even high surface area materials are formed of well defined cubic crystals with {100} as the dominant facets.[105] On the atomic level these surfaces consist of flat planes which have the bulk stoichiometry and so are charge neutral and have no dipole perpendicular to the surface plane. A zero dipole moment has been shown to lead to surface stability on electrostatic grounds.[106]

Table 4 Adhesion energies calculated for Au atoms on MgO surface. All values in eV

Method[a]	O_{5c}[b] top	Hollow[b]	Mg_{5c}[b] top	O_{4c}[c] (step)	O_{3c}[d] (kink)	F_s	F_s^+	Ref.
RPBE/USPP	0.57	0.44	0.31	—	—	—	—	121
PW91/USPP	0.88	0.72	0.51	—	—	—	—	121
PW91/PAW	0.89	—	—	1.26	—	3.17	3.97	119
PBE/TM/DZP	0.78	0.61	0.36	—	1.08	2.83	—	29

[a] Functional/pseudopotential type, all calculations used a planewave basis set except the final entry for which a double zeta plus polarisation (DZP) Gaussian basis was employed. [b] Standard sites on the flat MgO(100) surface. [c] Step site on MgO (310). [d] Kink site on MgO(1 3 10).

Cleavage of the MgO(100) surface removes one neighbour from each ion in the bulk, exposing five co-ordinate cations (Mg_{5c}) and anions (O_{5c}) in a checkerboard pattern. The adhesion energy, E_{adh}, for an Au atom or particle at a given site can be calculated in a similar manner to the adsorption energies for molecules to clusters:

$$E_{\mathrm{adh}} = -E(\mathrm{Au}_n/\mathrm{MgO}) + E(\mathrm{Au}_n) + E(\mathrm{MgO}) \qquad (3)$$

Where each term refers to the calculated energy for the system indicated. As in the case of adsorption energies, the reference energies $E(\mathrm{Au}_n)$ and $E(\mathrm{MgO})$ must be carrier out at the same level of theory and accuracy as the calculation for the total system. Using this definition, positive adhesion energy implies that the combined Au/MgO model has a lower calculated total energy than the sum of the two components. Table 4 gives some example data for Au atoms adsorbed to MgO surfaces. We have followed the convention that adhesion energies are reported in eV units. On the flat MgO(100) surface all calculations show that the highest adhesion energies are achieved for Au above the O_{5c} anions. The interaction has been characterised as a polarisation effect in which the Au atom is polarised by the anion field with only a minor degree of charge transfer.[107] The adhesion of Au to the surface in this way is weak and the diffusion of the atomic species around the surface is expected to be facile, leading to easy sintering of catalyst particles on the flat {100} terraces.[108] The calculated energies allow some further comparison of methodology to be made. For Au at O_{5c} sites the PW91 results with USPP representation of core states and those using the PAW approach are in excellent agreement. However, the PW91 tendency to overbind is evident, with the RPBE E_{adh} value some 0.31 eV below that for PW91. The PBE values are intermediate, about 0.1 eV below the PW91 results. Even so, all three functionals give the same ordering of the three MgO(100) sites considered.

Adsorption of Au at the low co-ordination oxygen sites presented by step edges (O_{4c}) or kinks (O_{3c}) are around 0.3 eV lower in energy than on the terrace, indicating that trapping of Au atoms at steps is likely on surfaces free of other defects.[29] For Au_{10} clusters, this mode of adsorption is found to be competitive with anchoring at point defects on the Mg(100) terraces.

In the model systems used in surface science experiments, MgO is grown as an ultra-thin film over an Mo substrate.[109,110] Recent calculations suggest that the presence of Mo increases the adhesion of Au to the support through an increased basicity of the oxide. This arises from alignment of the Fermi levels at the two metal/oxide interfaces.[111] Frondelius *et al.*[112] used the RPBE functional to compare the adhesion of Au_1–Au_6 on a 3 layer model of MgO with that for 3 layers of MgO overlaid on metallic Mo. For adsorption on the simple oxide, adhesion energies are relatively weak (0.6 to 1.4 eV), in line with the earlier results given in Table 4. For clusters of Au atoms there is no particular particle size dependence in the E_{adh} values and the planar structured particles prefer low co-ordination to the surface (one or two

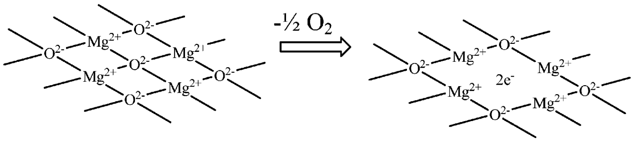

Fig. 15 Schematic illustration of the creation of an anion vacancy of MgO(100).

Au atoms in contact). There is also only minor charge transfer from the oxide to Au.

In contrast, with the Mo supported substrate, adhesion is enhanced by up to 1.5 eV with transfer of negative charge of around $-1|e|$ from the oxide to the Au clusters. For ultra-thin MgO layers the high electron affinity of Au will also facilitate electron tunnelling from the Mo metal through the insulating oxide; another possible mechanism for negative charging of Au particles in these experiments.[113] For Au on the MgO(100)/Mo substrate, the highest adhesion energy occurs on the hollow site and clusters with all Au atoms in contact with the surface are preferred over the minimal contact alternatives found for the MgO film alone. The enhancement effect in E_{adh} is seen to vary with the number of Au atoms present, so that odd numbered clusters are stabilised to a greater extent than even numbered, in line with the higher electron affinities of the former in the neutral cluster state. Further calculations on this system suggest that the negative charge will produce a core level energy shift of 1.9 eV in the Au(4f) shell, which may be detectable by XPS.[114]

The low adhesion of Au on the stoichiometric MgO(100) surface suggests that the experimentally-observed stable particles must be anchored to some surface defect. The most widely studied defect in oxides is the simple anion vacancy, denoted F_s. It is this type of vacancy that is generated by electron bombardment of MgO films. In the rock salt structured MgO the loss of an anion can be thought of as the creation of a defect generating $1/2O_2$(g) as illustrated in Fig. 15. In this process the two electrons of the anion are left behind and must be accommodated by the lattice. MgO is a wide band gap insulating material, which means that the energy gap, E_G, between the occupied valence states (formed largely from O orbitals) and the unoccupied conduction band states (which are the empty outer atomic orbitals of the Mg^{2+} cations) is quite large (Expt: 7.8 eV, PW91[115]: 5.2 and B3LYP[55]: 7.3). To place the excess electrons in the conduction band, and so partially reduce the cations, would require an energy on the order of E_G and so MgO is effectively an irreducible oxide. When an anion defect is formed in such a material the excess electrons are held at the F_s vacancy site by the Madelung potential of the ionic lattice and the corresponding energy levels appear as gap states.[116] In the F_s^+ centre only a single electron remains in the vacancy. To model this structure using periodic boundary conditions requires some care, since the cell must maintain charge neutrality. A simple way to generate a charge neutral feature with a similar electronic structure is to replace the Mg^{2+} cation at the base of the defect (in the second atomic layer of the surface) with a Na^+ cation.

The picture of vacancy formation on the flat MgO(100) surface has recently been refined by Pacchioni and co-workers.[105] Using a combination of electron paramagnetic resonance measurements and DFT calculations they point out that the energy to create an anion vacancy is much lower on the low co-ordination sites of step edges than on the {100} planes in which anions and cations are five co-ordinate.[117] However the majority of studies of Au supported on MgO anion defects have used the simpler model of the O_{5c} vacancy on MgO(100) as a model of the support. The columns headed F_s and F_s^+ in Table 4 refer to adsorption of an Au atom at these anion point defects. Adsorption at the F_s and F_s^+ defects give much higher adhesion energies than any of the stoichiometric surface sites. This enhanced adsorption at F_s centres on MgO(100) is also seen for other metals.[118] Placing an Au atom at the F_s^+ centre is found to be some 0.8 eV more favourable than at the F_s point defect. For the F_s^+ centre the strength of the interaction arises from a two electron bond formed between the Au atom and the surface through pairing of the single 6s electron of Au and the single electron in the defect.[119]

Donation of electron density from the defect to Au gives rise to negative Au atoms or particles at either defect site. However the effect on geometry and the spreading of the cluster charge is not the same as for the charging seen in the MgO/Mo support system. The localised nature of the F_s centre means that the bonding interaction involves the atom in the cluster that is directly over the defect to a much greater extent than the other Au atoms. The charge density difference for the Au(7,3) cluster on an F_s centre is shown in Fig. 16.[120] The contours on this diagram show the regions in which charge has been displaced relative to the charge density of the isolated surface and cluster. This allows the movement of charge due to bonding between the two components in the simulation to be emphasised. The central atom of the 7 atom layer (actually labelled 7 in Fig. 16) is immediately over the defect site. A Bader charge analysis of the total density shows a total charge on the Au cluster of $-2.194\ |e|$, and Table 5 shows that this charge is mainly held by the Au atoms in contact with the oxide surface, particularly Au number 7.

We have seen from the cluster calculations that O_2 adsorption is enhanced on negatively charged Au clusters while CO adsorption is weakened this distribution of the negative charge in the Au_{10} cluster would suggest that O_2 adsorption should occur at the base of the cluster near to the oxide surface while CO adsorbs more favourably on the low co-ordination top sites.

Extended models of the Au/MgO interface

Molina and Hammer have developed a series of models to study CO oxidation for Au supported on defect free MgO(100) using periodic RPBE and PW91 calculations and ultrasoft pseudopotentials.[121] Working with the large unit cell required to simulate an isolated cluster on an oxide surface is very computationally-demanding. Molina and Hammer make a compromise in which the edge of a cluster in contact with the oxide support is reproduced by having a rod like structure of Au which is periodic in one of the surface vector directions, as shown in Fig. 17. The bulk Au parameter is 4.08 Å, close to the MgO cubic unit cell (4.20 Å) and so only a 3% strain is required for epitaxy between Au(100) and MgO(100). This allows Au atoms

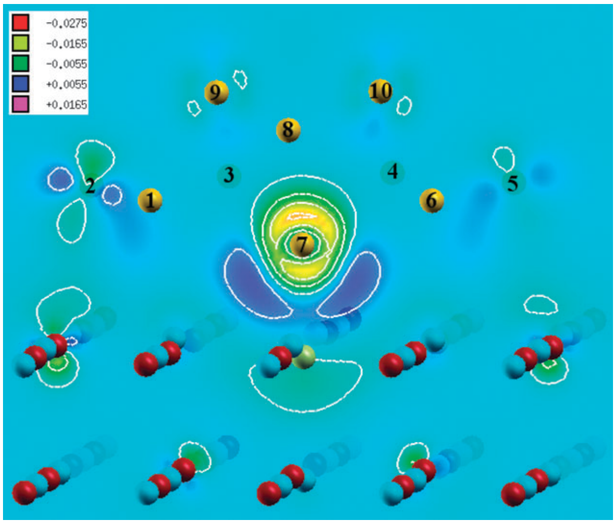

Fig. 16 Charge density difference for the $Au_{10}(7,3)$ cluster adsorbed on an F_s centre on MgO(001). Red/green colours represent charge depletion and blue/purple colours, charge accumulation. Lines are drawn in intervals of 0.005 e a_0^{-3}. Oxygen atoms in red, magnesium in blue, Au atoms are numbered and a single green centre in the defect is used to locate additional basis functions. Calculation using the PBE functional with TM style pseudopotentials in periodic calculation with a Gaussian DZP basis set, and a supercell consisting of a 3-layer slab with (8 × 8) surface cell, containing 192 Mg/O atoms. From ref. 120.

Table 5 Breakdown of the Bader charges for the $Au_{10}(7,3)$ cluster adsorbed in its semi-dodecahedral geometry on an MgO(100) F_s centre. Data for the lower layer atoms is in bold. Atoms numbered according to Fig. 16. The calculated total charge for Au_{10} is -2.194 $|e|$. Data taken from ref. 29

Gold atom	Charge ($|e|$)	Gold atom	Charge ($|e|$)
1	**−0.206**	**6**	**−0.182**
2	**−0.244**	**7**	**−0.947**
3	**−0.155**	8	−0.061
4	**−0.118**	9	−0.007
5	**−0.251**	10	−0.023

to be placed in registry with O_{5c}^{2-} ions on the oxide surface, as suggested by the results for atomic Au in Table 4.

To predict the most relevant edge structures to construct, the interfacial energies were calculated for a series of Au particles and Au monolayer (ML) on oxide systems. Even in the most favourable case, 2 ML film at PW91 level, the adhesion energy is low (0.31 eV per Au atom). This implies that, on defect free MgO(100), 3D growth of the Au cluster is preferred over 2D *i.e.* Au–Au interactions are more important than are $Au\cdots O_{5c}^{2-}$. So, for the larger nanoparticles represented by these periodic models, 3D structures will have lower energies than planar alternatives. A Wulff construction was used in this work to estimate the optimal particle shape based on a balance of surface and interfacial energies, as shown in Fig. 18. The particle is orientated with Au(100) parallel to the oxide surface to exploit the epitaxy mentioned above. However, the major facets are Au(111) which is more densely packed, and so has a lower surface energy. Transmission electron microscopy images of Au/MgO(100)[122] and on Au/TiO_2(110), have shown particles with similar shapes.

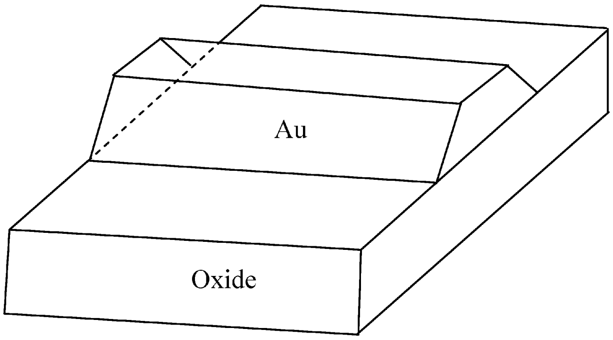

Fig. 17 Schematic illustration of a slab model with Au rods. The Au rod provides a model for the Au/oxide interface with a smaller simulation cell than would be required for a large Au particle. The Au atoms in the rod are always under a degree of strain due to the need for epitaxy with the oxide lattice in the direction of the rod axis.

For very small cluster sizes the Wulff plot becomes unreliable as specific interactions of corner and edge sites with the oxide, that are ignored in the surface energy argument, become significant. Calculations with an Au_{34} cluster showed that a truncated polyhedra is preferred over the particle shape suggested by the Wulff procedure. A series of periodic models using the rod geometry of Fig. 17 were then constructed to mimic the shape of the edge of the Wulff plot generated clusters and the edge of the Au_{34} pyramid for smaller clusters. We will return to the simulation of the catalytic oxidation of CO using these models in section 6.

TiO_2 supported Au

Titanium dioxide with the rutile structure has a preferred surface cleavage plane with the Miller indices (110). The relationship of this plane to the bulk unit cell is shown in Fig. 19. In the bulk all Ti atoms are six co-ordinate and all O ions three co-ordinate. The Ti centred octahedra can be thought of as edge sharing in rows with the octahedra of adjacent rows at right angles to one another. Each O ion is then bridging two Ti within a row, so is shared in the equatorial plane, and is acting as an axial neighbour of a Ti cation in an adjacent row. Cutting the unit cell parallel to the (110) plane at the position indicated in Fig. 19a, severs only axial Ti–O interactions. This exposes five co-ordinate Ti cations (Ti_{5c}) and two co-ordinate bridging oxygen ions (O_{2c}) at the surface, in a cell with surface vectors of a = 2.959 Å and b = 6.497 Å, based on the experimental structure. This termination has a particularly low surface energy and corresponds to the dominant facet of rutile phase TiO_2. To

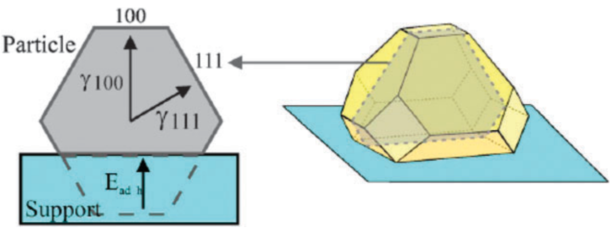

Fig. 18 The particle shape proposed for Au/MgO(100) based on surface and interface energies. From ref. 121. Copyright (2004) by the American Physical Society.

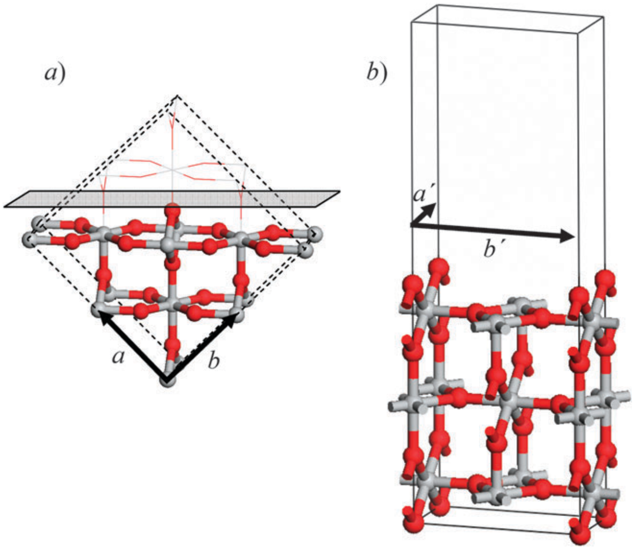

Fig. 19 (a) A $(2 \times 2 \times 1)$ supercell of TiO_2 showing the plane used to cut the $TiO_2(110)$ surface, the standard *a* and *b* vectors are shown, *c* is side of the cell pointing into the page. (b) A 3D periodic slab model for the simulation of the $TiO_2(110)$ surface, the 3D cell has been re-defined from the bulk so that $a' = c$ and $b' = a–b$, three tri-layers of O–Ti–O are shown. Atom colours: Ti light and O dark spheres.

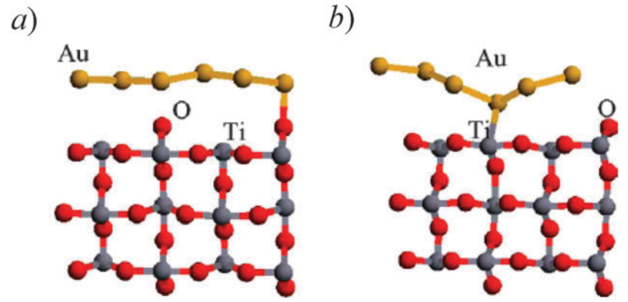

Fig. 20 Calculated structures for an Au(111) layer over (a) stoichiometric $TiO_2(110)$ and (b) partially reduced $TiO_2(110)$ formed by removing every other row of O_{2c} bridging anions. Reprinted from ref. 127, Copyright (2004), with permission from Elsevier.

simulate this surface a non-polar slab representation can be generated by taking an alternative setting of the lattice vectors. The desired face is used as the *ab*-plane and then a vacuum gap inserted in the *c*-direction to create a slab of material. A three layer slab for the $TiO_2(110)$ surface is shown in Fig. 19b.

Calculations comparing different adsorption sites show that the stoichiometric $TiO_2(110)$ surface has a very low affinity for Au.[123,124] In a PBE study of Au atoms adsorbed to the (2×4) surface using seven layer slabs Okazaki *et al.*[125] compared five alternative positions. Monolayer coverage is used in this study, meaning that there is one Au atom per (1×1) surface cell, giving a minimum Au···Au spacing of around 2.959 Å based on the surface cell of Fig. 19b. This ensures that all Au atoms are in equivalent surface environments and their separation is still larger than the 2.88 Å Au···Au distance in bulk Au. However, the rectangular shape of the surface cell means that strips of interacting Au are effectively created. At this surface density the highest adhesion energy is for the Au atoms over Ti_{5c} sites. At the lower coverage of one Au atom per (2×2) cell placing Au over the O_{2c} site is preferred. However, for either coverage, the adhesion energy values obtained are small; only 0.1 eV for the (1×1) case. Correspondingly, virtually zero charge transfer occurs between Au and the surface and the main interaction appears to be due to Au polarisation by the cation field, reminiscent of the defect free Au/MgO(100) case. An earlier report of an adhesion energy of 1.49 eV for Au at the same site by Yang *et al.*[126] was obtained under the local density approximation without gradient corrections which is known to lead to considerable overestimation of bond strengths. Both studies find only small changes to the electronic structure of the TiO_2 slab, indicative of weak binding.

Lopez *et al.*[127] have considered the interaction of a single atomic layer of Au(111) with $TiO_2(110)$ using a three layer slab model and the PW91 gradient corrected functional. The main goal is to investigate the adhesion of the Au layer, representing the base of a large Au particle, to the surface. Stoichiometric and oxygen deficient slab models of the support were compared. The introduction of the layer and the placement of defects on only one side of the slab generates an electric dipole across the simulation cell perpendicular to the surface. This can lead to artefacts as the interaction between dipoles is quite long range and so the influence of dipolar periodic images must be taken into account. This is quite a common problem and so methods have been developed to impose a counteracting field and so restore the potential of the isolated surface.[128] For the clean stoichiometric surface they find a negligibly small interaction between the layer of Au and the surface. Fig. 20a shows the resulting structure has the Au layer quite distant from the surface which is unperturbed by its presence. To study the effect of surface reduction, defects were introduced by removing alternate rows of surface O_{2c} ions. The removal of surface oxygen on a reducible oxide generates quite different electronic states to the F_s centres discussed for MgO. Formally, the Ti centres near to the defect site will take up the electrons left by the O_{2c} and be reduced to Ti^{3+}. At the GGA-DFT level this results in electrons occupying the bottom of the conduction band. This is largely due to the self-interaction problem in GGA-DFT which leads to an underestimation of the band gaps of oxides and favours de-localised solutions. This arises because of each electron contributes to the density used to evaluate its own potential. In transition metal oxides methods to compensate for the self interaction, such as DFT + U, can show charge localisation at reduced metal centres.[69] Similarly hybrid-DFT methods like B3LYP have been shown to localise charge at Ti_{6c} sites near to the O_{2c} defect on $TiO_2(110)$,[129] although these have not yet been applied to the study of metal adatoms.

In the study of Lopez *et al.*[127] the interaction energy of the Au layer with the reduced surface was estimated to be 1.6 eV per defect. This leads to the conclusion that Au particles will be pinned at defect sites on $TiO_2(110)$ and so the dispersion of metal particles will be directly related to the defect concentration. Similar differences in the calculated binding energy of Au particles on the stoichiometric and those on the reduced (101) surface of the anatase form of TiO_2 have also been found.[130] Lopez *et al.*[127] also developed a morphology model based on a Wulff construction using surface and interface energies. They propose that the thermodynamically preferred particle shape for

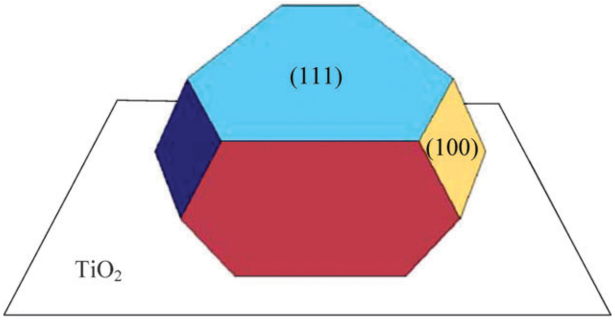

Fig. 21 The particle shape proposed for Au/TiO_2(110) based on surface and interface energies. Reprinted from ref. 127, Copyright (2004), with permission from Elsevier.

Au on defective TiO_2(110) is flat; consisting of 3–4 atomic layers of Au with a diameter of 3 nm, and having an acute contact angle with the oxide as shown in Fig. 21. This reflects the higher interfacial energy in this system compared to the defect free MgO(100) example of Fig. 18 for which near hemi-spherical particle shapes are predicted.

In Okazaki's work the group went on to consider "Ti rich" surfaces in which the bridging oxygen atoms of one side of the slab are removed.[125] This is equivalent to shifting the plane used to cut the surface in Fig. 19a downward, so that the Ti_{6c} atoms are exposed as Ti_{4c} sites. The Ti rich surface is effectively reduced by the removal of the bridging oxygen atoms and at the GGA-DFT level this results in electrons occupying the bottom of the conduction band. On this surface Au atoms adsorb to the vacant O_{2c} sites and electrons are transferred from the Ti_{4c} ions to give negatively charged Au species with an adhesion energy of 1.90 eV per adatom with respect to a free Au monolayer. Okazaki and co-workers have also considered Au adsorption to an "O rich" TiO_2(110) surface.[131] Here the O_{2c} atoms are again removed but in addition the Ti_{6c} cations underlying them are also deleted. This gives an over-oxidised surface with a missing formal charge of $+2$ per defect site, the opposite of the "Ti rich" case. Now the Au atoms form cationic like species in the vacant Ti_{6c} sites with adhesion energies of 4.50 eV. The structures generated on the "O rich" surface compare well with Au particles deposited by the wet chemistry deposition precipitation method examined using electron holography. The images show particles similar in shape to those predicted using interfacial energies by Molina and Hammer (Fig. 18) for Au/MgO(100). Similar trends in adhesion energy with surface stoichiometry were also found for Pt on TiO_2(110) by the same group.[132]

These studies of surface adhesion highlight the dependency of the types of Au species present in experimental work on the preparation methods used. On the stoichiometric surface, in common with MgO(100), adhesion is weak and particle agglomeration should be expected. For the small particle sizes required for active catalysts some sort of defect anchoring is required. The majority of studies have concentrated on reduced TiO_2(110) and shown that small anionic Au clusters can be stabilised. The donation of charge from the reduced oxide surface appears to be more complex than for the F_s centre on MgO. A recent study by Chrétien and Metiu[133] using a PW91 functional and plane wave basis suggests that charging of Au_n (n = 1–7) clusters will occur if the lowest unoccupied molecular orbital (LUMO) of the gas phase cluster is orientated toward a Ti_{5c} surface ion. They find that even if the Ti_{5c} atom is quite remote from the defect charging will occur. Although this effect may be due to the GGA-DFT delocalisation of the defect charge in the TiO_2 conduction band discussed earlier.

These reduced surfaces are most likely relevant to the clusters formed under ultra-high vacuum conditions. However Okazaki has shown that on over oxidised surfaces cationic Au species are even more strongly bound and suggests that these are more relevant to the materials produced by the deposition precipitation route. Cationic Au has not received the same theoretical attention as anionic species. This may be because the models required have to consider a wider range of surface structures, due to the uncertain nature of the accompanying anion. In a recent study by Phala *et al.*, for example, cationic Au species were studied on the formally dipolar surface of ZnO using an embedded cluster methodology and a large core ECP for Au.[134] To generate an effectively non-polar surface cation vacancies are introduced which make natural adsorption sites for Au species. Thermodynamic arguments including the ionisation potential of Au are used to show that both Au^0 and Au^I can be stabilised at these cation vacancies but higher oxidation states cannot. However, if the oxidation state is promoted by the addition of anions to form neutral Au species $Au(OH)_2$ and $Au(OH)_3$ adhesion energies of 2.66 and 4.84 eV, respectively are found. Direct ion exchange with surface Zn^{2+} (as implied by Ozakaki's oxygen rich termination of TiO_2) was not found to be favourable when a full thermodynamic cycle was considered.

6. Adsorption and reaction of CO and O_2 on oxide supported Au particles

MgO supported Au

The adsorption of CO to an Au atom positioned over an O_{5c} ion on MgO(100) has been studied recently by Risse and co-workers.[135] They show that PW91, B3LYP and CCSD(T)

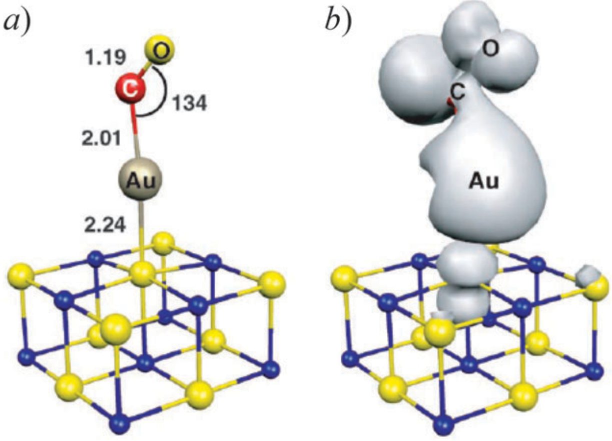

Fig. 22 (a) The adsorption geometry and (b) calculated spin density for CO adsorbed to a single Au atom over an O site on MgO(100). The examples shown are at the PW91 level. From ref. 135. Copyright (2006) Wiley-VCH Verlag GmbH & Co. KGaA. Reproduced with permission.

calculations all give similar geometries for the adsorbate with an Au–C–O angle of around 134° as shown in Fig. 22a. As was seen for the isolated Au atoms and clusters (*e.g.* Fig. 8), this configuration allows the electron donation from Au into the CO anti-bonding $2\pi^*$ orbital. In fact, for this Au/MgO(100) calculation, the CO stretching frequency is found to be strongly red-shifted compared with the gas phase reference calculation, by 298 cm^{-1} for the CCSD(T) calculation. This gives an estimated frequency of 1863 cm^{-1}, which is in much closer agreement with the entry for CO bonded to isolated Au^- in Table 2 than with the entry for a charge neutral Au atom. We have seen that calculations of Au on the stoichiometric MgO(100) surface suggest a weak interaction with little charge transfer to the Au atom. Risse and co-workers suggest that the Lewis acid nature of CO causes the electron withdrawal from the O_{5c} surface ion, so that, in the presence of CO, the Au atom becomes negatively charged. This bonding picture is confirmed the spin density plot in Fig. 22b which shows that the O_{5c} ion directly under the Au atom is no longer closed shell. This effect is likely to be most pronounced in situations where the interaction of Au with the oxide is initially weak. However, it does bring into question the use of CO as an "innocent" probe in experiments to quantify the charge state of surface adsorbed Au.

The Au only calculations summarised in Table 3 suggest that single Au atoms in any charge state are unlikely to lead to activated di-oxygen species and so the majority of work in the simulation of the CO oxidation reaction has considered some model of a gold particle. Molina and Hammer's work with periodic Au rod models and an Au_{34} cluster on the defect free MgO(100) surface indicates that CO adsorption on corner and edge sites is much stronger than on face sites, which hardly bind CO at all.[121] Corner sites near the MgO surface are also disfavoured due to steric repulsion between CO and oxide surface. The highest binding energy for CO is found at a corner site in the second layer of the three layer cluster with a binding energy of 48 kJ mol^{-1}. In contrast, di-oxygen adsorption is estimated to be slightly endothermic at the RPBE level and slight exothermic with the PW91 functional. The adsorption of O_2 in all stable geometries has the axis of the molecule parallel to the oxide surface and bridging two Au atoms, a $\mu_{1,1}$ mode in the notation of Table 3. The O_2 molecule is adsorbed in a superoxo state with a bond length enlarged from 1.24 Å, in a reference gas phase calculation, to 1.35 Å. The calculated magnetic moment, of 0.8 μ_B, is also consistent with this assignment of a superoxo adsorption mode. Dissociation of O_2 is endothermic unless the adsorption sites for the resulting O atoms are at the Au strip/oxide interface, binding to a low co-ordination Au atom and a substrate Mg_{5c}^{2+} cation. In this case the $O\cdots Mg_{5c}^{2+}$ distance is 2.20 Å, close to the 2.15 Å O^{2-}–Mg^{2+} nearest neighbour separation in the bulk MgO reference calculation. However, the barrier to O_2 dissociation, at the most favourable adsorption site, is still significant, (106 kJ mol^{-1} (PW91) and 164 kJ mol^{-1} (RPBE)). The dissociation of oxygen prior to CO oxidation (*i.e.* Scheme 1) is thus difficult to rationalise with the low reaction barriers to CO oxidation observed experimentally. To proceed Molina and Hammer note that the co-adsorption of O_2 and CO at the Au/oxide interface can give a high adsorption energy for an $O_2\cdots CO$ dimer of up to 74 kJ mol^{-1}, depending on structure of the interface. A species also identified in the calculations of CO oxidation over Au/TiO_2 by Rodriguez and co-workers.[136] The most favourable geometries found by Molina and Hammer allow the O_2 molecule to straddle the Au/oxide interface interacting with both Au atoms in the cluster base and an oxide Mg_{5c} site. They propose that reaction is initiated in an Eley–Rideal process in which gas phase O_2 is captured by pre-adsorbed CO into this type of dimer, skipping step (i) of Scheme 2. An example interface and dimer structure (shown with dotted atoms) is reproduced in Fig. 23. The solid atoms in the Figure show the transition state geometry for O_2 moving from the gas phase directly into the dimer state. This process has a low barrier of only 14 kJ mol^{-1} with the RPBE functional, and is barrierless at the PW91 level. Progression to CO_2 from this proposed intermediate involves only low barriers, as noted from the cluster calculations discussed earlier. The atomic oxygen remaining after the first liberation of CO_2 is also able to oxidise further CO. This model provides a pathway with low barriers to CO oxidation, but its efficiency will clearly be limited by the formation of the $O_2\cdots CO$ surface dimer which can only occur at the Au/oxide interface.

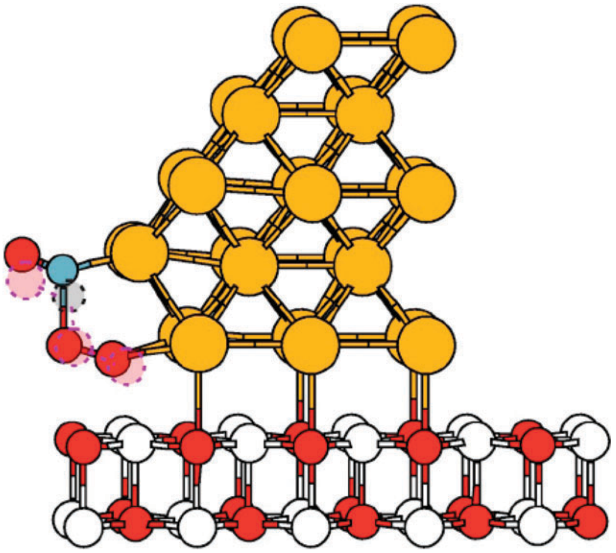

Fig. 23 An $O_2\cdots CO$ dimer at an Au/MgO interface modelled using the Au rod approach (Fig. 17). The molecules shown with solid lines represent the transition state at the RPBE level for O_2 moving from the gas phase to form a dimer with pre-adsorbed CO. The final state is shown with dotted lines. From ref. 121. Copyright (2004) by the American Physical Society.

Oxygen adsorption at negatively charged clusters is more favourable, certainly for the isolated clusters of Table 3. Even numbered anionic clusters give the highest O_2 adsorption energies due to Au_n^-–O_2 bonds in which the unpaired electron is donated to an O_2 anti-bonding orbital. Häkkinen and co-workers[101] have considered the oxidation of CO catalysed by $Au_8(5,3)$ clusters supported at an F_s centre on MgO(100). They use the PBE functional and TM style pseudopotentials with a large core for Au. The calculations use an embedded cluster approach in which the central region is treated at the full DFT level while lattice sites more remote from the Au cluster are represented as point charges. The binding energy of the cluster to the surface F_s centre in this model is some 3.45 eV.[137] The $Au_8(5,3)$ cluster has one atom directly over the defect site and the expected negative charge transfer is seen. The pattern of distribution of this donated charge around the cluster is similar to the Au_{10}(7,3) case illustrated in Fig. 16, *i.e.* the atoms in the layer at the oxide interface carry the majority of the charge.

However, the Au_8 cluster is small enough that an O_2 molecule adsorbed at the interface can be co-ordinated to the Au atom immediately over the F_s centre. At the PBE level stronger binding of O_2 to Au_8/MgO(F_s) is found than to Au_8/MgO (45 *cf.* 29 kJ mol^{-1}), with the peroxy species preferred for the cluster at the F_s centre (d(O_2) = 1.42 Å) while the stoichiometric support gives the less activated superoxo (d(O_2) = 1.35 Å).[11] The charge transfer from the defect centre to the Au particle enhances the adsorption of oxygen because there is correspondingly greater donation into the $2\pi_u$* orbital of the molecule. The overall charge on comparable Au_8/O_2/CO system is reported to be −0.87 |*e*| on the stoichiometric MgO(100) surface and −1.58 |*e*| in the presence of the F_s centre. The adsorption of CO occurs at an atom in the top layer of Au_8 in the presence of the O_2 at the cluster base with the F_s centre supported cluster now giving weaker adsorption of CO, E_{ads} = 63 kJ mol^{-1} compared to 76 kJ mol^{-1} when a non-defective support is used. Correspondingly, the calculated vibrational frequency of CO is 34 cm^{-1} lower for the F_s centre supported cluster.

In the parallel surface science experiments using defective MgO as a support $^{13}C^{16}O$ is reacted with $^{18}O_2$ and the products monitored by mass spectrometry in temperature programmed reaction experiments.[101] Only $^{13}C^{16}O^{18}O$ is seen in the product CO_2, indicating that there is no exchange of the oxygen atom in CO, nor introduction of lattice oxygen into the reaction. They also use this observation to rule out carbonate as a possible intermediate. At very low temperatures (140 K) oxidation of CO at a small number of sites is seen. Their earlier calculations within the local spin density approximation[79] indicated that an O_2 molecule adsorbed to the top face of the Au_8 cluster at the F_s centre is activated to a peroxy species and is able to react directly with gas phase CO, in an Ely–Rideal fashion, without a barrier. At higher temperatures O_2 is only adsorbed at the Au/MgO interface.

TiO_2 supported Au

The methodology described for Au/MgO(100) systems has also been applied to Au supported on TiO_2(110). The Au interface with the stoichiometric surface has been considered by Liu *et al.*[138] using a similar supported rod approach to Molina and Hammer (Fig. 17). The PBE functional is used along with a localised basis set in a periodic boundaries simulation. They chose to use a two layer strip of Au since the surface science experiments of Goodman and co-workers have suggested high activity for such metal bi-layers.[139] The surface of TiO_2 is non-planar due to the lines of bridging O_{2c} atoms (Fig. 19b) and the Au strip does not conform to the shape of the oxide surface. This means that, while the minimum Au···O_{2c} separation is 2.2 Å, the closest Au···Ti_{5c} distance is some 3.9 Å, and is consistent with the weak interaction picture for the fully oxidised TiO_2 slab in Fig. 20. The adsorption energy for O_2 to this Au rod model without the inclusion of the TiO_2 slab is negligible (7 kJ mol^{-1}). However with the slab in place O_2 adsorbs quite strongly, with E_{ads} = 83 kJ mol^{-1}. In the resulting geometry the O_2 molecule is on top of a Ti_{5c} cation in a η^2 co-ordination mode and simultaneously interacting with the Au strip with $\mu_{1,1}$ co-ordination across a Au–Au bridge site. The O–O distance has also elongated to 1.46 Å compared to the reference gas phase calculated value of 1.24 Å and there is no net magnetic moment, suggesting a peroxy anion O_2^{2-} like state. A charge density analysis confirms occupancy of the $2\pi_u$* O_2 molecular orbital (MO) and Mulliken analysis gives an estimated molecular charge of 0.72*e*. It is suggested that the charge moves exclusively from the Au strip to the O_2 molecule, and that this is made easier by the local electric field of the Ti_{5c} cation which lowers the energy of the $2\pi_u$* MO with respect to the Au Fermi level. Dissociation of O_2 at this site involves a barrier of only 50 kJ mol^{-1}, making CO oxidation by surface atomic O (Scheme 1) a viable mechanism.

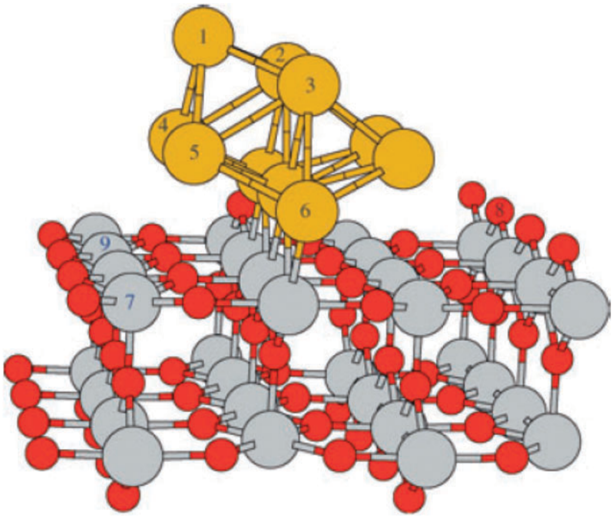

Fig. 24 The relaxed geometry for Au_{10} supported at O_{2c} defect sites on TiO_2(110). From ref. 140. Copyright (2005) Wiley-VCH Verlag GmbH & Co. KGaA. Reproduced with permission.

The high affinity of Au monolayers for the reduced TiO_2(110) surface noted earlier has led to calculations for Au on the sub-stoichiometric surface. Removing three bridging O_{2c} atoms from the surface Remediakis *et al.*[140] considered the reactivity of an Au_{10} cluster for CO oxidation. After relaxation of all the Au atoms using the RPBE functional and ultrasoft pseudopotentials the three atoms in the cluster that are closest to the O_{2c} vacancies remain bonded to the surface, as shown in Fig. 24. However, the Au cluster is distorted away from the Au(7,3) shape of Fig. 5, with the other four base layer Au atoms moving away from the surface. Despite this distortion the cluster retains atoms in co-ordination geometries typical of the Au(111) and Au(100) surfaces. As was seen for clusters deposited on defective MgO(100), the cluster is negatively charged when supported on this oxygen deficient surface. Charge density plots also show that the Au atoms in contact with the oxide carry the bulk of the additional electron density.

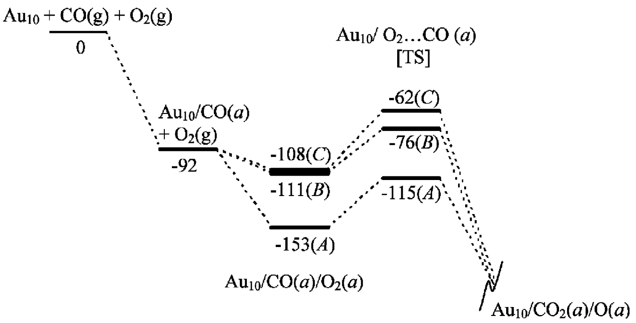

Fig. 25 Comparison of potential energy schemes for CO oxidation on (A) Au_{10} supported on reduced TiO_2(110) with O_2 adsorbing at interface, (B) Au_{10} supported on reduced TiO_2(110) with O_2 adsorbing away from interface and (C) isolated Au_{10} cluster.

With this cluster a strong O_2 binding site, consisting of a corner gold atom and a neighbouring Ti_{5c} site, is found. The co-adsorption energy for O_2 at this site and CO bound to the uppermost Au atom (labelled 1 in Fig. 24) is 153 kJ mol^{-1}. For the same geometry of cluster in the absence of the oxide support the co-adsorption energy drops to 108 kJ mol^{-1}. The energy pathway for CO oxidation was compared for three model systems designed to highlight the influence of the metal/oxide interface and the support effect on the Au cluster properties:

(A) The supported Au_{10}/TiO_2(110) catalyst with O_2 initial adsorption at the particle/oxide interface. This structure has O_2 stabilised through co-ordination to Au atoms in the base of the cluster and a neighbouring Ti_{5c} ion.

(B) The supported Au_{10}/TiO_2(110) catalyst with O_2 initial adsorption away from the particle/oxide interface. To obtain this structure a geometric constraint was imposed to prevent the optimisation moving the O_2 molecule to the interface region. This gives an energy low enough to be involved in the reaction schemes and it is argued that on the larger particles low co-ordination sites more remote from the oxide surface would be available.

(C) The Au_{10} cluster was considered in isolation. To keep the geometry of the free cluster close to that of the supported one, the three atoms formerly in contact with the oxide were held fixed during optimisations.

The energy profiles for these three schemes are compared in Fig. 25. The adsorption energy of CO on the top site showed only a weak dependence on the model used giving E_{ads} = 92 kJ mol^{-1}. This is in reasonable agreement with experimental measurements of CO binding to supported Au clusters by Meier and Goodman who report 77 kJ mol^{-1} for a 1.8 nm Au cluster on TiO_2.[141]

Pathway A gives the most stable O_2 adsorption energy of 61 kJ mol^{-1} relative to the supported cluster with CO pre-adsorbed. The adsorption of O_2 away from the interface (B) or to the free cluster (C) gives much lower E_{ads} values, 19 and 16 kJ mol^{-1}, respectively. These estimates suggest that pathways (B) and (C) may only be significant at low temperatures but that the interface region is able to stabilise oxygen adsorption to higher temperatures through co-ordination to exposed surface cations. The reaction barriers for all three pathways are in the range expected from experimental kinetics.[90] The lowest barrier is found for route B (35 kJ mol^{-1}) but this is only 4 kJ mol^{-1} higher than that for O_2 starting from the interface region in pathway A. The highest barrier is found for the free Au_{10} cluster which, at 46 kJ mol^{-1}, is comparable with this group's earlier work on the rigid Au_{10}(7,3) cluster.[54] The comparison of the three pathways does suggest that the negative charging of the cluster by adsorption at the bridging oxygen defect leads to a barrier reduction of around 7 kJ mol^{-1}.

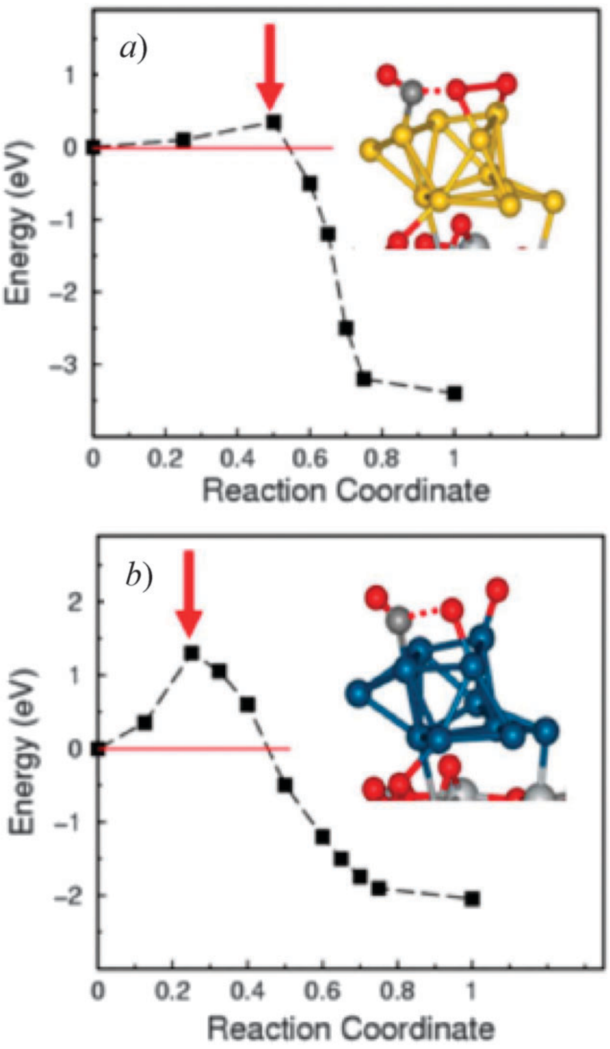

Fig. 26 Nudged elastic band calculations for the barrier of the CO oxidation step for (a) a Au cluster and (b) a Pt cluster on TiO_2(110). From ref. 142. Copyright (2007) by the American Physical Society.

Rashkeev *et al.*[142] have used the PBE functional to compare CO oxidation over Au clusters supported at a bridging oxygen defect on TiO_2(110) and the same structures with Au atoms replaced by Pt. They point out that the small particle sizes required for Au catalysis actually lead to a degradation in the performance of Pt. Cluster sizes were gradually built up using a bridging oxygen defect as an anchor point. This creates a series of models with sites of differing metal co-ordination. On Pt they find that O_2 adsorbed to the top of a typical cluster has a low barrier to dissociation, so that the active oxidising species is atomically adsorbed O, whereas on Au molecularly adsorbed O_2 is preferred in agreement with earlier calculations. The barrier to CO oxidation in each case was calculated using the nudged elastic band method.[143] Here a series of structures are constructed along the reaction pathway which then have all other degrees of freedom simultaneously optimised. Along the reaction co-ordinate direction each image is held in place by constraint forces determined by its position relative to neighbouring images (the "elastic band" forces). Convergence of the set of images gives an estimate for a low energy pathway between the end points, so that the reaction barrier can be estimated from the maximum point along this pathway. Typical results from Rashkeev *et al.*[141] are shown in Fig. 26. These reaction profiles, involving adsorbates on Au sites away from the oxide interface, show that the barrier to produce CO_2 on Au is lower than on Pt. However, the low adsorption energy of O_2 on Au means that reaction is only preferred over desorption if Au sites with co-ordination numbers lower than 5 are available. On Pt, reaction is always more favourable than desorption, even at sites with CN = 9 in the Pt(111) faces of large particles. Adsorption of O_2 at the Au/oxide interface increases the barrier to desorption so that reaction is favoured even for Au sites with CN = 6 or 7. The inset pictures of the transition state geometries in Fig. 26 also show that the response of the metal particles to the presence of the adsorbates is quite different. In Au the metal···metal bonds are weakened while in the Pt cluster appears to become more tightly packed and so quite rigid. The authors suggest that this is linked to the fluxionality of the particles so that Au clusters react more readily during the course of the reaction which may be a factor in the observed relatively low reaction barrier.

Water and the supported Au catalyst models

With the introduction of the oxide support the role for water adsorbed to the oxide should also be considered as a possible explanation of the rate acceleration observed when H_2O is present during the CO oxidation reaction.[91,92] Hu and co-workers have argued that, even with favorable O_2 adsorption at perimeter sites, the reaction should become starved of O_2 since the reservoir maintained by such adsorption will be quite low.[144] For a supported catalyst it is also feasible that O_2 adsorption on the oxide surface provides a supply of molecular oxygen to the Au particles through surface diffusion. This source of oxygen is one possible explanation for the switch over in apparent activation energy reported by Haruta.[145] Below 200 K O_2 has been shown to adsorb favorably at bridging oxygen defects on $TiO_2(100)$, of the type invoked to anchor Au particles. However, calculations suggest that the activation energy to leave the defect is too great to allow diffusion to the Au sites to take part in CO oxidation.[146] Hu and co-workers[143] point out that if these defects are instead blocked by water dissociation the defects will be only be partially healed as illustrated in Fig. 27a. The water dissociation replaces the missing O_{2c} with an OH group, protonating a neighboring O_{2c}. The presence of defects of this type implies that the surface is still reduced although there are no oxygen vacancy sites. Using PBE calculations in a periodic plane wave basis model Hu considers a surface with a single OH group to mimic this kind of semi-healed surface, effectively replacing $O_{2c}{}^{2-}$ with $(OH)_{2c}{}^{-}$ at one site. He finds that the excess electron moves onto the Ti_{5c} sites, rather than the Ti_{6c} ions indicated in the scheme of Fig. 27a. A density difference map, $\rho(H/TiO_2)-\rho(H)-\rho(TiO_2)$, indicates that this electron is delocalised along the entire row of 8 Ti_{5c} in the $p(1 \times 8)$ simulation cell (Fig. 27b). Adsorbing an O_2 molecule over the Ti_{5c} site nearest to the bridging OH results in a favourable binding to the oxide surface. At low OH coverage (1/8 ML) the O_2 bond length increases from 1.24 Å, calculated for gas phase O_2, to 1.32 Å, with an accompanying magnetic moment decrease to $1.0\mu_B$, consistent with partial electron transfer from the surface to give a superoxo species. The negatively charged di-oxygen species is then bound to the exposed Ti_{5c} cations. The adsorption energy of O_2 to this surface is 77 kJ mol^{-1} near to the defect, compared with practically zero for the clean stoichiometric surface.

The effect is also found to be quite long range because the additional electron is spread over several Ti_{5c} sites (Fig. 27b). This facilitates diffusion of molecular oxygen along the Ti_{5c} rows with a barrier of only 0.19 eV. A possible role for water in these reactions is to increase the capture zone around the particles for molecular oxygen and to allow its easy transport to the Au clusters where reaction with CO can take place.

However, at the same time that Hu's paper was published, Pacchioni and co-workers[147] showed that, at the hybrid DFT level, the defect states at an O_{2c} vacancy healed by dissociative H_2O adsorption has states in the band gap, Fig. 27c. The corresponding spin density shows that these states correspond to single Ti^{3+} species at Ti_{6c} and Ti_{5c} locations, *i.e.* the electrons localise at particular Ti sites. Morgan and Watson have recently shown similar charge localisation in the vicinity of the O_{2c} vacancy itself using the DFT + U method.[148] The differences in the calculated charge densities between these methods and GGA-DFT arise because of the self interaction problem in GGA-DFT which favours delocalised states, as mentioned earlier. In hybrid DFT the contribution from exact exchange alleviates this problem and so electron localisation is described more easily. There is a similar debate regarding the localisation of electrons at anion defects on TiO_2 in the experimental literature. Electron paramagnetic resonance shows the creation of localised Ti^{3+} sites,[149] while vibrational analysis of TiO–H stretching modes for TiO_2 (anatase) gives seems to indicate electron de-localisation.[150]

Even so, we would expect the "true" picture to involve more localisation of the electrons than GGA-DFT suggests. The hybrid calculations still show the preference for an excess electron to reside on a Ti_{5c} site and so O_2 adsorption should be promoted, but probably not with the same long range effect found in the GGA-DFT simulations.

7. Environmental effects on Au surfaces

The models presented up to this point have taken a wholly atomistic modeling approach in which the effective concentration of the reactants in the gas phase is zero. This gives adsorption energies and structures in the low pressure limit, one reason why the comparison of the calculations with surface science experiments under ultra-high vacuum seems

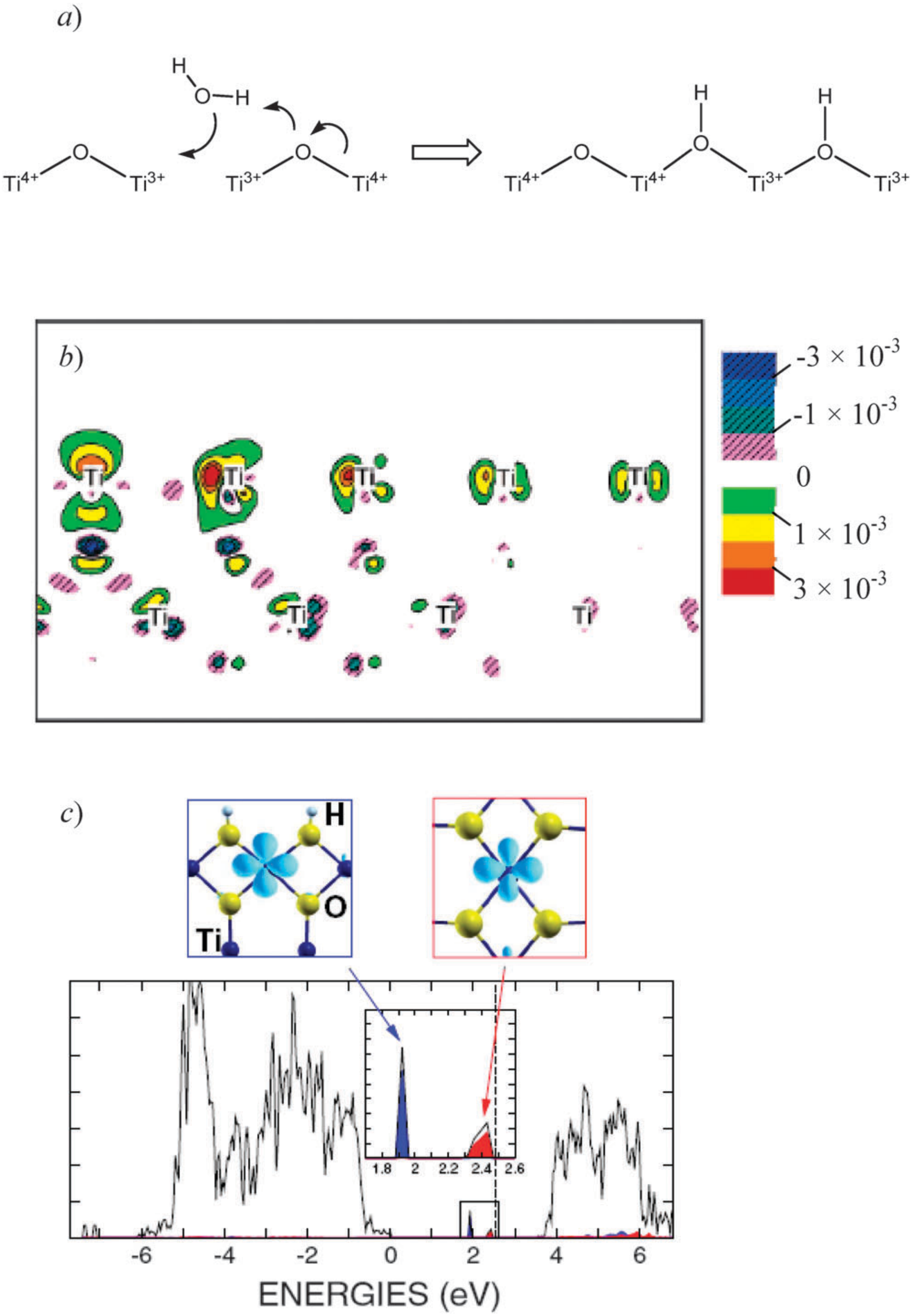

Fig. 27 (a) Schematic mechanism of H_2O dissociation at an O_{2c} vacancy site on $TiO_2(110)$. (b) Calculated charge density difference along a row of Ti_{5c} atoms in the $TiO_2(110)$ when a single O_{2c} atom is replaced by OH in a $p(1 \times 8)$ cell. The Ti site to the far left of the diagram is at the cell centre and nearest to the OH group. Only one half of the row is shown, the density difference is symmetrical, centred on the Ti site nearest the defect. Reprinted with permission from ref. 144. Copyright 2006 American Chemical Society. (c) The density of states and spin density for the defect resulting from H_2O dissociation at an O_{2c} vacancy on $TiO_2(110)$ at the hybrid DFT level, gap states corresponding to localised Ti^{3+} centres are obtained. From ref. 147. Copyright (2006) by the American Physical Society.

excellent. Under these conditions a reduced oxide support gives negatively charged Au particles which are capable of adsorbing molecular oxygen to take part in the oxidation reaction. If the oxide is not reduced the affinity for oxygen is low and O_2 must be captured directly into an $O_2 \cdots CO$ intermediate. Calculations on single O_2 molecules over Au surfaces show that the barrier to dissociation is much weaker than that to desorption, making O_2 activation to form surface atomic oxygen unfavourable. However for ordered mono-layer oxides on high index metal surfaces, such as Au(321), calculations suggest that the energy of the oxide layer can be favourable with respect to gas phase O_2.[151]

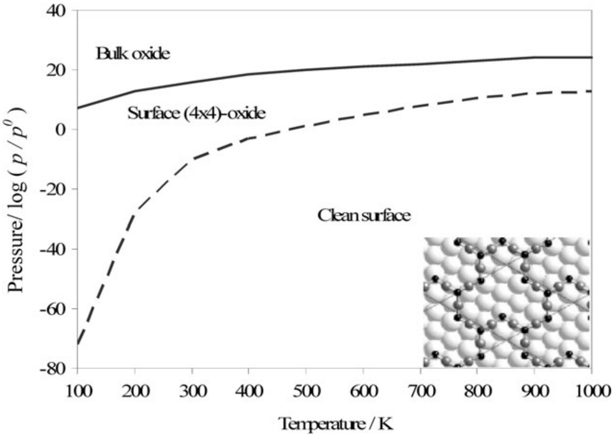

Fig. 28 Phase stability diagram for Au surface oxide (structure shown as inset) and bulk Au_2O_3 as a function of temperature and pressure. From ref. 153. Copyright (2007) by the American Physical Society.

Extensions of the single molecule adsorption picture are now being put forward that allow interpolation of the results to O_2 vapour pressures that are relevant to the active catalyst under practical operating conditions. The idea is to evaluate the stability of these surface oxides in the operating environment of a working catalyst. The link is made *via* the chemical potential of oxygen, which can be used to give the free energy of adsorbed atomic oxygen:

$$\Delta G(T,P) = \frac{N}{A}\left(-E_{\mathrm{ads}} - \mu_{\mathrm{O}}(T,P^{\mathrm{O}}) - \frac{1}{2}kT\ln\left(\frac{P}{P^{\mathrm{O}}}\right)\right) \quad (4)$$

N is the number of oxygen atoms and A the surface area per unit cell. E_{ads} is the calculated adsorption energy per oxygen atom calculated relative to an O_2(g) reference state following eqn (2). The chemical potential of oxygen, μ_{O}, as a function of temperature, T, and oxygen partial pressure, P^{O}, is available in standard tables of thermodynamic data. This approach can be used to predict the thermodynamically preferred surface composition of a metal catalyst as a function of oxygen partial pressure. For example, Reuter and Scheffler have shown how RuO_2(110) moves from an over oxidised state for high O chemical potential to a reduced form at the lower end of the accessible range.[152] Shi and Stampf[153] have considered a number of models for a surface oxide on Au(111). The most stable consists of a thin surface layer in which O is co-ordinated by three Au atoms and each Au atom is linearly co-ordinated to two oxygen atoms in an incomplete hexagonal array with a $p(4 \times 4)$ surface unit cell. This arrangement is shown as an inset Fig. 28, oxygen atoms bonded to three surface Au atoms are over hollow sites while those with only two surface Au interactions are also associated with a Au atom in the underlying Au(111) surface. The graph of Fig. 28 shows that this surface oxide is thermodynamically stable up to around 500 K at normal pressures, whereas bulk Au_2O_3 is not.

Laursen and Linic have used similar thermodynamic arguments to consider an Au bi-layer adsorbed to reduced TiO_2(110) and to a model SiO_2(110)-rutile surface, to give a comparable irreducible support with the same atomic geometry. Under low pressure conditions $Au^{\delta-}$ is the favored species, but as the oxygen chemical potential is adjusted to reflect atmospheric pressure the Au layer is oxidised to give $Au^{\delta+}$. The switch over point occurs at lower O chemical potential on TiO_2(110) than on the reference SiO_2 surface.

8. Conclusions

Gold catalysis continues to be an exciting and expanding area of research. From a theoretical standpoint the small particle size and important support effects stretch the available computing power and the accuracy of the GGA-DFT approximation. For example, in predicting the shapes of Au clusters in isolation the dispersion force appears to be important in determining the cluster size at which 2D planar structures give way to 3D. Usually the 3D structures are also minima on the GGA-DFT energy surface and so can be used in simulations of adsorption and reaction.

Calculations on isolated Au clusters and periodic models of high index bulk surfaces allow general observations to be made that do seem to carry over to supported catalyst particles. Carbon monoxide adsorbs strongly to low co-ordination Au atoms in Au_n^0 and $Au_n{}^+$ particles and to a lesser extent at anionic clusters, although adsorption energies are still in the range 80–110 kJ mol^{-1}. Bonding of CO to Au involves an electrostatic interaction and donation from the metal to the anti-bond $2\pi^*$ molecular orbital. Given that the highest occupied orbital of Au^0 is 6s this leads to non-linear Au–C═O geometries in neutral and anionic clusters.

The adsorption of O_2 in molecular form seems to require an unpaired electron from the metal particle and, preferably, an anionic Au species. This ties in with the well known variation of apparent electron affinity with metal atom number in Au clusters. For the smallest clusters a non-linear η^1 structure similar to that for CO occurs, but for the larger particles a bridging $\mu_{1,1}$ geometry generally gives a lower adsorption energy. Donation from the metal into the $2\pi_u{}^*$ molecular orbital in this case leads to superoxo or peroxy anions. However, dissociative adsorption (while thermodynamically preferred) has a kinetic barrier higher than that for O_2 desorption.

The advantage of mechanisms invoking Au adsorbed to reduced oxide surfaces is the enhanced adsorption of molecular O_2 due to the negatively-charged cluster. We have seen from cluster calculations that anionic clusters generally bind CO less strongly than the neutral or cationic counterparts. However, the localised nature of the charging in the defect supported clusters means that the top layer Au atoms are still close to charge neutral and so give sites suitable for CO adsorption. A small particle size ensures a high density of these complementary adsorption sites are close enough together for a reaction to take place.

On reduced oxide surfaces there is clearly good agreement between surface science experiments and calculations. The negatively charged metal particles can adsorb and activate O_2 near to the metal/oxide interface where electron density is accumulated. Capture of CO on top sites leads to oxidation through a $O_2\cdots CO$ intermediate (Scheme 2). The role of the support in these calculations is to charge the Au clusters and potentially, in the case of TiO_2, to provide a greater reservoir of oxidant. This is one possible explanation for the higher activity of Au supported on reducible compared with irreducible supports. Water may also act here to increase the affinity of the oxide surface for molecular O_2.

The possible catalytic role of cationic species, which is often implied from experimental data, has not been studied as intensively as negatively charged clusters by the DFT modeling fraternity. Although, Phala *et al.*[134] found CO adsorption to Au(I) on ZnO to be more favourable than on Au(II) or Au(III), with E_{ads} = 143, 49 and 56 kJ $\mathrm{mol^{-1}}$, respectively. Surface oxides of Au may also give an alternative interpretation of the experimental observation of cationic Au in working catalysts. These oxides are unlikely candidates as an oxygen source: The large barriers to O_2 dissociation found in most calculations on Au would suggest that any thin surface oxide would be quickly exhausted in the early stages of reaction and not efficiently replenished. However, if the surface oxide is stable under reaction conditions, the cationic Au species it contains should be considered as possible participants in CO oxidation with molecular oxygen.

Oxygen activation requires electron donation to weaken the O_2 bond. The results for small positively charged particles in Table 3 suggest that cationic Au would not be able to adsorb or activate O_2 effectively. However, the calculations on the charge distributions in Au particles adsorbed at negatively charged defects clearly show that the negatively charged Au atoms are near the interface. The counter anions for cationic Au particles are likely to adsorb near the metal/oxide interface where co-ordination to surface cations of the oxide is also possible. By analogy with the anionic cluster work this may mean that particles with cationic character at the periphery, but near-charge-neutral top sites could be constructed. These have been suggested from experimental workers. The Bond–Thompson[154] and Kung models[155] rely on cationic Au species at the base of particles that also contain metallic Au. In the Kung model O_2 is adsorbed dissociatively to the Au^0 region of the cluster while CO adsorbs at a cationic Au site forming a hydroxycarbonyl species with the OH^- counter anion. The surface atomic oxygen is then used to oxidise the hydroxycarbonyl to bicarbonate which then decomposes to CO_2, restoring the surface OH^- anion. The Bond–Thompson model invokes O_2 adsorption at oxide lattice defects near to the Au particle/oxide interface. These mechanisms are more complex than the Au only, or anionic cluster models discussed in the main part of this review, but they do take into account the main components of the catalysts prepared by wet chemistry that are thought to be important for CO oxidation. In the future, testing and adaptation of these models by first principles calculations will be key to further unravelling the details of the fascinating heterogeneous catalysis of gold.

References

1 M. Haruta, N. Yamada, T. Kobayashi and S. Iijima, *J. Catal.*, 1989, **115**, 301.
2 G. J. Hutchings, *J. Catal.*, 1985, **96**, 292.
3 P. Landon, J. Ferguson, B. E. Solsona, T. Garcia, A. F. Carley, A. A. Herzing, C. J. Kiely, S. E. Golunski and G. J. Hutchings, *Chem. Commun.*, 2005, 3385.
4 D. Cameron, R. Holliday and D. Thompson, *J. Power Sources*, 2003, **118**, 298.
5 A. S. K. Hashmi and G. J. Hutchings, *Angew. Chem., Int. Ed.*, 2006, **45**, 7896.
6 R. Meyer, C. Lemire, S. K. Shaikhutdinov and H.-J. Freund, *Gold Bull.*, 2004, **37**, 72.
7 M. M. Schubert, S. Hackenberg, A. C. van Veen, M. Muhler, V. Plzak and R. J. Behm, *J. Catal.*, 2001, **197**, 113.
8 M. Mavrikakis, P. Stoltze and J. K. Nørskov, *Catal. Lett.*, 2000, **64**, 101.
9 N. Lopez, T. V. W. Janssens, B. S. Clausen, Y. Xu, M. Mavrikakis, T. Bligaard and J. K. Nørskov, *J. Catal.*, 2004, **223**, 232.
10 B. Hvolbæk, T. V. W. Janssens, B. S. Clausen, H. Falsig, C. H. Christensen and J. K. Nørskov, *Nano Today*, 2007, **2**, 14.
11 A. Sanchez, S. Abbet, U. Heiz, W.-D. Schneider, H. Häkkinen, R. N. Barnett and U. Landman, *J. Phys. Chem. A*, 1999, **103**, 9573.
12 Y. Chen, P. Crawford and P. Hu, *Catal. Lett.*, 2007, **119**, 21.
13 P. Pyykkö, *Chem. Rev.*, 1988, **88**, 563.
14 P. Pyykkö, *Angew. Chem., Int. Ed.*, 2004, **43**, 4412.
15 P. Pyykkö, *Inorg. Chim. Acta*, 2005, **358**, 4113.
16 For introductory material on relativisitic methods see: F. Jensen, *Introduction to Computational Chemistry*, Publ. John Wiley & Sons Ltd., 2nd edn, 2007, Ch. 8, ISBN: 10 0-470-01186-6.
17 P. A. M. Dirac, *Proc. R. Soc. London, Ser. A*, 1928, **A117**, 610.
18 O. Kullie, H. Zhang, J. Kolb and D. Kolb, *J. Chem. Phys.*, 2006, **125**, 244303.
19 E. van Lenthe, E. J. Baerends and J. G. Snijders, *J. Chem. Phys.*, 1993, **99**, 4597.
20 E. van Lenthe, E. J. Baerends and J. G. Snijders, *J. Chem. Phys.*, 1994, **101**, 9783.
21 P. H. T. Philipsen and E. J. Baerends, *Phys. Rev. B*, 2000, **61**, 1773.
22 M. C. Payne, M. P. Teter, D. C. Allan, T. A. Arias and J. D. Joannopoulos, *Rev. Mod. Phys.*, 1992, **64**, 1045.
23 M. J. Frisch, G. W. Trucks, H. B. Schlegel, G. E. Scuseria, M. A. Robb, J. R. Cheeseman, J. A. Montgomery, Jr., T. Vreven, K. N. Kudin, J. C. Burant, J. M. Millam, S. S. Iyengar, J. Tomasi, V. Barone, B. Mennucci, M. Cossi, G. Scalmani, N. Rega, G. A. Petersson, H. Nakatsuji, M. Hada, M. Ehara, K. Toyota, R. Fukuda, J. Hasegawa, M. Ishida, T. Nakajima, Y. Honda, O. Kitao, H. Nakai, M. Klene, X. Li, J. E. Knox, H. P. Hratchian, J. B. Cross, V. Bakken, C. Adamo, J. Jaramillo, R. Gomperts, R. E. Stratmann, O. Yazyev, A. J. Austin, R. Cammi, C. Pomelli, J. Ochterski, P. Y. Ayala, K. Morokuma, G. A. Voth, P. Salvador, J. J. Dannenberg, V. G. Zakrzewski, S. Dapprich, A. D. Daniels, M. C. Strain, O. Farkas, D. K. Malick, A. D. Rabuck, K. Raghavachari, J. B. Foresman, J. V. Ortiz, Q. Cui, A. G. Baboul, S. Clifford, J. Cioslowski, B. B. Stefanov, G. Liu, A. Liashenko, P. Piskorz, I. Komaromi, R. L. Martin, D. J. Fox, T. Keith, M. A. Al-Laham, C. Y. Peng, A. Nanayakkara, M. Challacombe, P. M. W. Gill, B. G. Johnson, W. Chen, M. W. Wong, C. Gonzalez and J. A. Pople, *GAUSSIAN 03 (Revision C.02)*, Gaussian, Inc., Wallingford, CT, 2004.
24 P. J. Hay and W. R. Wadt, *J. Chem. Phys.*, 1985, **82**, 270.
25 P. J. Hay and W. R. Wadt, *J. Chem. Phys.*, 1985, **82**, 299.
26 D. Figgen, G. Rauhut, M. Dolg and H. Stoll, *Chem. Phys.*, 2005, **311**, 227.
27 K. A. Peterson and C. Puzzarini, *Theor. Chem. Acc.*, 2005, **114**, 283.
28 W. J. Stevens, M. Krauss, H. Basch and P. G. Jasien, *Can. J. Chem.*, 1992, **70**, 612.
29 R. Coquet, G. J. Hutchings, S. H. Taylor and D. J. Willock, *J. Mater. Chem.*, 2006, **16**, 1978.
30 N. Troullier and J. L. Martins, *Phys. Rev. B*, 1991, **43**, 1993.
31 S. Scandolo, P. Giannozzi, C. Cavazzoni, S. de Gironcoli, A. Pasquarello and S. Baroni, *Z. Kristallogr.*, 2005, **220**, 574.
32 D. Vanderbilt, *Phys. Rev. B*, 1990, **41**, 7892.
33 P. E. Blöchl, *Phys. Rev. B*, 1994, **50**, 17953.
34 G. Kresse and D. Joubert, *Phys. Rev. B*, 1999, **59**, 1758.
35 J. P. Perdew, in *Electronic Structure of Solids*, ed. P. Ziesche and H. Eschrig, Publ. Akademie Verlag, Berlin, 1991.
36 J. P. Perdew, J. A. Chevary, S. H. Vosko, K. A. Jackson, M. R. Pederson, D. J. Singh and C. Fiolhais, *Phys. Rev. B*, 1992, **46**, 6671.
37 A. D. Becke, *Phys. Rev. A*, 1988, **38**, 3098.
38 C. Lee, W. Yang and R. G. Parr, *Phys. Rev. B*, 1988, **37**, 785.
39 J. P. Perdew, K. Burke and M. Ernzerhof, *Phys. Rev. Lett.*, 1996, **77**, 3865.

40 Y. Zhang and W. Yang, *Phys. Rev. Lett.*, 1998, **80**, 890.
41 B. Hammer, L. B. Hansen and J. K. Nørskov, *Phys. Rev. B*, 1999, **59**, 7413.
42 A. D. Becke, *J. Chem. Phys.*, 1993, **98**, 5648.
43 Y.-f. Zhang, W. Lin, Y. Li, K.-n. Ding and J.-q. Li, *J. Phys. Chem. B*, 2005, **109**, 19270.
44 F. Cora, M. Alfredsson, G. Mallia, D. S. Middlemiss, W. C. Mackrodt, R. Dovesi and R. Orlando, in *Principles and Applications of Density Functional Theory in Inorganic Chemistry II: Structure and Bonding*, Publ. Springer-Verlag, Berlin, 2004, vol. 113, p. 171.
45 K. Balasubramanian and M. Z. Liao, *J. Chem. Phys.*, 1987, **86**, 5587.
46 X. Wu, L. Senapati, S. K. Nayak, A. Selloni and M. Hajaligol, *J. Chem. Phys.*, 2002, **117**, 4010.
47 L. Xiao, B. Tollberg, X. Hu and L. Wang, *J. Chem. Phys.*, 2006, **124**, 114309.
48 J. A. Howard, R. Sutcliffe and B. Mile, *Surf. Sci.*, 1985, **156**, 214.
49 R. Guo, K. Balasubramanian, X. Wang and L. Andrews, *J. Chem. Phys.*, 2002, **117**, 1614.
50 K. Taylor, C. Pettiette-Hall, O. Cheshnovsky and R. Smalley, *J. Chem. Phys.*, 1992, **96**, 3319.
51 H. Häkkinan and U. Landman, *Phys. Rev. B*, 2000, **62**, 2287R.
52 R. M. Olson, S. Varganov, M. S. Gordon, H. Metiua, S. Chretien, P. Piecuch, K. Kowalski, S. A. Kucharski and M. Musial, *J. Am. Chem. Soc.*, 2005, **127**, 1049.
53 F. Cosandey, L. Zhang and T. E. Madey, *Surf. Sci.*, 2001, **474**, 1.
54 I. N. Remediakis, N. Lopez and J. K. Nørskov, *Appl. Catal., A*, 2005, **291**, 13.
55 J. Muscat, A. Wander and N. M. Harrison, *Chem. Phys. Lett.*, 2001, **342**, 397.
56 K. Okazaki, S. Ichikawa, Y. Maeda, M. Haruta and M. Kohyama, *Appl. Catal., A*, 2005, **291**, 45.
57 O. D. Häberlen, S.-C. Chung, M. Stener and N. Rösch, *J. Chem. Phys.*, 1997, **106**, 5189.
58 A. S. Barnard and L. A. Curtiss, *ChemPhysChem*, 2006, **7**, 1544.
59 A. S. Goldman and K. Krogh-Jespersen, *J. Am. Chem. Soc.*, 1996, **118**, 12159.
60 F. B. van Duijneveldt, J. G. C. M. van Duijneveldt-van de Rijdt and J. H. van Lenthe, *Chem. Rev.*, 1994, **94**, 1873.
61 M. Okumura, Y. Kitagawa, M. Haruta and K. Yamaguchi, *Appl. Catal., A*, 2005, **291**, 37.
62 B. Liang and L. Andrews, *J. Phys. Chem. A*, 2000, **104**, 9156.
63 H. Häkkinen and U. Landman, *J. Am. Chem. Soc.*, 2001, **123**, 9704.
64 D. W. Yuan and Z. Zeng, *J. Chem. Phys.*, 2004, **120**, 6574.
65 P. J. Feibelman, B. Hammer, J. K. Nørskov, F. Wagner, M. Scheffler, R. Stumpf, R. Watwe and J. Dumesic, *J. Phys. Chem. B*, 2001, **105**, 4018.
66 D. F. Ogletree, M. A. Van Hove and G. A. Somorjai, *Surf. Sci.*, 1986, **173**, 351.
67 G. Kresse, A. Gil and P. Sautet, *Phys. Rev. B*, 2003, **68** 073401.
68 Z.-P. Liu, P. Hu and A. Alavi, *J. Am. Chem. Soc.*, 2002, **124**, 14770.
69 R. Coquet and D. J. Willock, *Phys. Chem. Chem. Phys.*, 2005, **7**, 3819.
70 D. A. Outka, J. Stöhr, W. Jark, P. Stevens, J. Solomon and R. J. Madix, *Phys. Rev. B*, 1987, **35**, 4119.
71 K. P. Huber and G. Herzberg, in *Molecular Spectra and Molecular Structure*, Van Nostrand Reinhold, New York, 1979.
72 G. Mills, M. S. Gordon and H. Metiu, *Chem. Phys. Lett.*, 2002, **359**, 493.
73 X. Ding, Z. Li, J. Yang, J. G. Hou and Q. Zhu, *J. Chem. Phys.*, 2004, **120**, 9594.
74 S. A. Varganov, R. M. Olson, M. S. Gordon and H. Metiu, *J. Chem. Phys.*, 2003, **119**, 2531.
75 W. T. Wallace, A. J. Leavitt and R. L. Whetten, *Chem. Phys. Lett.*, 2003, **368**, 744.
76 D. H. Wells, Jr, W. N. Delgass and K. T. Thompson, *J. Catal.*, 2004, **225**, 69.
77 A. M. Joshi, W. N. Delgass and K. T. Thompson, *J. Phys. Chem. B*, 2005, **109**, 22392.
78 D. H. Wells, Jr, W. N. Delgass and K. T. Thompson, *J. Chem. Phys.*, 2002, **117**, 10597.
79 B. Yoon, H. Häkkinan and U. Landman, *J. Phys. Chem. A*, 2003, **107**, 4066.
80 E. M. Fernández, P. Ordejón and L. C. Balbás, *Chem. Phys. Lett.*, 2005, **408**, 252.
81 B. E. Salisbury, W. T. Wallace and R. L. Whetten, *Chem. Phys.*, 2000, **262**, 131.
82 Y. Xu and M. Mavrikakis, *J. Phys. Chem. B*, 2003, **107**, 9298.
83 B. Hammer and J. K. Nørskov, *Nature*, 1995, **376**, 238.
84 A. Alavi, P. Hu, Th. Deutsch, P. L. Silvestrelli and J. Hutter, *Phys. Rev. Lett.*, 1998, **80**, 3650.
85 P. A. Gravil, D. M. Bird and J. A. White, *Phys. Rev. Lett.*, 1996, **77**, 3933.
86 A. Raukema, D. A. Butler and A. W. Kleyn, *J. Phys.: Condens. Matter*, 1996, **8**, 2247.
87 N. Lopez and J. K. Nørskov, *J. Am. Chem. Soc.*, 2002, **124**, 11262.
88 M. Olea and Y. Iwasawa, *Appl. Catal., A*, 2004, **275**, 35.
89 L. D. Socaciu, J. Hagen, T. M. Bernhardt, L. Wöste, U. Heiz, H. Häkkinen and U. Landman, *J. Am. Chem. Soc.*, 2003, **125**, 10437.
90 M. Haruta, S. Tsubota, T. Kobayashi, H. Kageyama, M. J. Genet and B. Delmon, *J. Catal.*, 1993, **144**, 175.
91 M. Daté, M. Okumura, S. Tsubota and M. Haruta, *Angew. Chem., Int. Ed.*, 2004, **43**, 2129.
92 C. K. Costello, J. Guzman, J. H. Yang, Y. M. Wang, M. C. Kung, B. C. Gates and H. H. Kung, *J. Phys. Chem. B*, 2004, **108**, 12529.
93 G.-C. Wang, S.-X. Tao and X.-H. Bu, *J. Catal.*, 2006, **244**, 10.
94 M. Okamura, M. Haruta, Y. Kitagawa and K. Yamaguchi, *Gold Bull.*, 2007, **40**, 40.
95 A. Bongiorni and U. Landman, *Phys. Rev. Lett.*, 2005, **95**, 106102.
96 Y. Iizuka, T. Tode, T. Takao, K. Yatsu, T. Takeuchi, S. Tsubota and M. Haruta, *J. Catal.*, 1999, **187**, 50.
97 F. Moreau, G. C. Bond and A. O. Turner, *J. Catal.*, 2005, **231**, 105.
98 F. Moreau and G. C. Bond, *Catal. Today*, 2007, **122**, 260.
99 J. Guzman and B. C. Gates, *J. Am. Chem. Soc.*, 2004, **126** 2672.
100 M. Yulikov, E. Fischbach, M. Heyde, H.-P. Rust, G. Pacchioni, T. Risse and H.-J. Freund, *Angew. Chem., Int. Ed.*, 2006, **45**, 2630.
101 B. Yoon, H. Häkkinan, U. Landman, A. S. Wörz, J.-M. Antonietti, S. Abbet, K. Judai and U. Heiz, *Science*, 2005, **307**, 403.
102 D. Alfè and M. J. Gillan, *J. Phys.: Condens. Matter*, 2006, **18**, L435.
103 S. J. Thompson and S. P. Lewis, *Phys. Rev. B*, 2006, **73**, 073403.
104 V. Swamy, J. Muscat, J. D. Gale and N. M. Harrison, *Surf. Sci.*, 2002, **504**, 115.
105 M. Chiesa, M. C. Paganini, E. Giamello, D. M. Murphy, C. Di Valentin and G. Pacchioni, *Acc. Chem. Res.*, 2006, **39**, 861.
106 C. Noguera, *J. Phys.: Condens. Matter*, 2000, **12**, R367.
107 I. Yudanov, G. Pacchioni, K. Neyman and N. Rösch, *J. Phys. Chem. B*, 1997, **101**, 2786.
108 A. Del Vitto, G. Pacchioni, F. Delbecq and P. Sautet, *J. Phys. Chem. B*, 2005, **109**, 8040.
109 M.-C. Wu, J. S. Corneille, C. A. Estrada, J.-W. He and D. W. Goodman, *Chem. Phys. Lett.*, 1991, **182**, 472.
110 C. Xu, W. S. Oh, G. Liu, D. Y. Kim and D. W. Goodman, *J. Vac. Sci. Technol., A*, 1997, **15**, 1261.
111 K. Honkala and H. Häkkinen, *J. Phys. Chem. C*, 2007, **111**, 4319.
112 P. Frondelius, H. Häkkinen and K. Honkala, *Phys. Rev. B*, 2007, **76**, 073406.
113 G. Pacchioni, L. Giordano and M. Baistrocchi, *Phys. Rev. Lett.*, 2005, **94**, 226104.
114 L. Giordano, U. Martinez, S. Sicolo and G. Pacchioni, *J. Chem. Phys.*, 2007, **127**, 144713.
115 T. Bredow and A. R. Gerson, *Phys. Rev. B*, 2000, **61**, 5194.
116 L. N. Kantorovich, J. M. Holender and M. J. Gillan, *Surf. Sci.*, 1995, **343**, 221.
117 E. Giamello, M. C. Paganini, D. M. Murphy, A. M. Ferrari and G. A. Pacchioni, *J. Phys. Chem. B*, 1997, **101**, 971.
118 Y. F. Zhukovskii, E. A. Kotomin and G. Borstel, *Vacuum*, 2004, **74**, 235.
119 A. Del Vitto, G. Pacchioni, F. Delbecq and P. Sautet, *J. Phys. Chem. B*, 2005, **109**, 8040.

120 R. Coquet, PhD thesis, Cardiff University, 2005.
121 L. M. Molina and B. Hammer, *Phys. Rev. B*, 2004, **69**, 155424.
122 B. Pauwels, G. Van Tendeloo, W. Bouwen, L. T. Kuhn, P. Lievens, H. Lei and M. Hou, *Phys. Rev. B*, 2000, **62**, 10383.
123 A. Vijay, G. Mills and H. Metiu, *J. Chem. Phys.*, 2003, **118**, 6536.
124 Y. Wang and G. S. Hwang, *Surf. Sci.*, 2003, **542**, 72.
125 K. Okazaki, Y. Morikawa, S. Tanaka and M. Kohyama, *Phys. Rev. B*, 2004, **69**, 235404.
126 Z. Yang, R. Wu and D. W. Goodman, *Phys. Rev. B*, 2000, **61**, 14066.
127 N. Lopez, J. K. Nørskov, T. V. W. Janssens, A. Carlsson, A. Puig-Molina, B. S. Clausen and J.-D. Grunwaldt, *J. Catal.*, 2004, **225**, 86.
128 J. Neugebauer and M. Scheffler, *Phys. Rev. B*, 1992, **46**, 16067.
129 T. Bredow and G. Pacchioni, *Chem. Phys. Lett.*, 2002, **355**, 417.
130 A. Vittadini and A. Selloni, *J. Chem. Phys.*, 2002, **117**, 353.
131 K. Okazaki, S. Ichikawa, Y. Maeda, M. Haruta and M. Kohyama, *Appl. Catal., A*, 2005, **291**, 45.
132 K. Okazaki, Y. Morikawa, S. Tanaka, K. Tanaka and M. Kohyama, *J. Mater. Sci.*, 2005, **40**, 3075.
133 S. Chrétien and H. Metiu, *J. Chem. Phys.*, 2007, **126**, 104701.
134 N. S. Phala, G. Klatt, E. van Steen, S. A. French, A. A. Sokol and C. R. A. Catlow, *Phys. Chem. Chem. Phys.*, 2005, **7**, 2440.
135 M. Sterrer, M. Yulikov, T. Risse, H.-J. Freund, J. Carrasco, F. Illas, C. Di Valentin, L. Giordano and G. Pacchioni, *Angew. Chem., Int. Ed.*, 2006, **45**, 2633.
136 N. C. Hernández, J. F. Sanz and J. A. Rodriguez, *J. Am. Chem. Soc.*, 2006, **128**, 15600.
137 H. Häkkinen, S. Abbet, A. Sanchez, U. Heiz and U. Landman, *Angew. Chem., Int. Ed.*, 2003, **42**, 1297.
138 Z.-P. Liu, X.-Q. Gong, J. Kohanoff, C. Sanchez and P. Hu, *Phys. Rev. Lett.*, 2003, **91**, 266102.
139 M. Valden, X. Lai and D. W. Goodman, *Science*, 1998, **281** 1647.
140 I. N. Remediakis, N. Lopez and J. K. Nørskov, *Angew. Chem., Int. Ed.*, 2005, **44**, 1824.
141 D. C. Meier and D. W. Goodman, *J. Am. Chem. Soc.*, 2004, **126**, 1892.
142 S. N. Rashkeev, A. R. Lupini, S. H. Overbury, S. J. Pennycook and S. T. Pantelides, *Phys. Rev. B*, 2007, **76**, 035438.
143 G. Mills, H. Jonsson and G. K. Schenter, *Surf. Sci.*, 1995, **324**, 305; H. Johnson, G. Mills and K. W. Jacobsen, in *Classical and Quantum Dynamics in Condensed Phase Systems*, ed. B. J. Berne, G. Cicotti and D. F. Coker, World Scientific, RiverEdge, NJ, 1998.
144 L. M. Liu, B. McAllister, H. Q. Ye and P. Hu, *J. Am. Chem. Soc.*, 2006, **128**, 4017.
145 M. Haruta, *CATTECH*, 2002, **6**, 102.
146 M. D. Rasmussen, L. M. Molina and B. Hammer, *J. Chem. Phys.*, 2004, **120**, 988.
147 C. D. Valentin and G. Pacchioni, *Phys. Rev. Lett.*, 2006, **97**, 166803.
148 B. J. Morgan and G. W. Watson, *Surf. Sci.*, 2007, **601**, 5034.
149 D. C. Hurum, A. G. Agrios, K. A. Gray, T. Rajh and M. C. Thurnauer, *J. Phys. Chem. B*, 2003, **107**, 4545.
150 S. H. Szczepankiewicz, J. A. Moss and M. R. Hoffmann, *J. Phys. Chem. B*, 2002, **106**, 7654.
151 J. L. C. Fajín, M. N. D. S. Cordeiro and J. R. B. Gomes, *Surf. Sci.*, 2008, **602**, 424.
152 K. Reuter and M. Scheffler, *Phys. Rev. B*, 2001, **65**, 035406.
153 H. Shi and C. Stampf, *Phys. Rev. B*, 2007, **76**, 075327.
154 G. C. Bond and D. T. Thompson, *Gold Bull.*, 2000, **33**, 41.
155 H. H. Kung, M. C. Kung and C. K. Costello, *J. Catal.*, 2003, **216**, 425.